AFFDL-TR-66-112

AERODYNAMIC NOISE SIMULATION IN SONIC FATIGUE FACILITY

RICHARD H. LYON, et al

BOLT BERANEK AND NEWMAN, INC.

FOREWORD

The research described in this report was conducted by Bolt Beranek and Newman, Inc., Cambridge, Massachusetts, for the Aero-Acoustics Branch, Vehicle Dynamics Division, AF Flight Dynamics Laboratory, Wright-Patterson Air Force Base, Ohio, under Contract AF33(615)-1290. The research performed is part of a continuing effort to provide improved techniques for noise simulation in the Sonic Fatigue Facility. This effort is part of the Research and Technology Division, Air Force Systems Command's exploratory development program. The contract was initiated under Project No. 4437 "High Intensity Sound Environment Simulation", Task No. 443701 "Sonic Fatigue Development". Messrs. A. W. Kolb and O. F. Maurer were the project engineers. The research was conducted during the period from 15 January 1964 to 15 April 1965.

This report was prepared by Richard H. Lyon, Colin G. Gordon, Raya Stern and Francis M. Wiener. Contractor's report number is 1349.

Manuscript was released by the authors in April 1966 for publication as an AFFDL Technical Report.

This technical report has been reviewed and is approved.

Walter J. Mykytow

WALTER J. MYKYTOW
Asst. for Research & Technology
Vehicle Dynamics Division

ABSTRACT

The possibility of simulating a turbulent boundary-layer noise environment using the air-flow capability of the RTD Sonic Fatigue Facility is investigated. The philosophy is adopted that it is the mechanical power absorbed by the structure from the environment that is to be duplicated. Calculations are developed that allow the prediction of the mechanical power injected into a structure by a turbulent boundary layer (TBL), and by a turbulent wall-jet. The possibility of replacing the power injected by the TBL by using turbulent wall-jets impinging on a structural model of a section of a supersonic transport is studied. Results indicate that high-frequency excitation (above 1 kHz) can be adequately simulated, but that the air-flow capabilities of the facility would be exceeded by an attempt to excite a structure as large as the one chosen by a set of wall-jets at lower frequencies.

TABLE OF CONTENTS

PART I STUDIES OF STRUCTURAL RESPONSE

LIST OF ILLUSTRATIONS

LIST OF ILLUSTRATIONS (continued)

LIST OF TABLES

LIST OF SYMBOLS

A	panel area
A_t, $A_{t(1)}$	correlation areas
c_B	bending wave speed
c_ℓ	longitudinal wave speed
d	pipe diameter
$\overline{df^2}$	differential mean-square force
dN	number of uncorrelated eddies in interval dR
D	mean free path of panel
E	Young's Modulus
E_i	plate modal energy
f	response frequency
f_{co}	cutoff frequency
f_h	hydrodynamic critical frequency
$f_{h\ell}$	approximate lower-frequency limit to HC excitation
$F(\omega)$	spectral density of the exciting power in the wall-jet
G_∞	transverse mechanical point input
H	function of $\omega\theta$, Eq. (2.10)
HC	hydrodynamically coincident
HF	hydrodynamically fast
HS	hydrodynamically slow
h	panel thickness
k	radial component of $\underset{\sim}{k}$
$\underset{\sim}{k}$	wavevector, conjugate to $\underset{\sim}{x}$

LIST OF SYMBOLS (continued)

k_d	constant of proportionality defined by Eq.(2.12)
k_p	free bending wavenumber for panel
k_1	component of wavevector in direction of convection
ℓ	flange-to-wall spacing
ℓ_3	transverse correlation scale for radial wall-jet
L_1, L_3	linear dimensions of panel
M	aircraft flight profile Mach number
n_i	modal density of i^{th} panel
N	number of identical wall-jets per system
p	pressure (positive in the direction of positive panel displacement)
p_h, $p_{h(1)}$	turbulent rms pressures
P	length of energy-transferring boundary
$\mathcal{P}(\underset{\sim}{k},\omega)$	spectrum of the transform of the correlation function $\overline{pp'}$
$\mathcal{P}_x(\underset{\sim}{k})$	wavevector spectrum, normalized to have unit area
$\mathcal{P}_3$	projection of $\mathcal{P}_x$ spectrum along k_3 axis
$\mathcal{P}_T(\omega)$	moving-axis frequency spectrum
q	dynamic pressure head
Q	average pipe volume flow
r_1	jet flange radius
r_2	equivalent outer radius of test panel
R, R_1	radial distances from wall-jet axis

LIST OF SYMBOLS (continued)

SST	supersonic transport
t, t'	time coordinates
T_R	reverberation time
TBL	turbulent boundary layer
U_c	convection speed
U_m	maximum velocity in wall-jet profile
U_1	air speed at position removed from panel
$\mathcal{U}(\omega)$	power spectral density of panel velocity
$\overline{v^2}$	measured mean-square velocity on panel
V	average pipe flow speed
x	distance along fuselage
$\underset{\sim}{x}$, $\underset{\sim}{x}_1'$; x_1, x_3; x_1', x_3'	space coordinates
y	transverse displacement of infinite panel
z_m	distance to velocity maximum U_m
$z_{1/2}$	distance to 1/2-velocity point (in the jet regime of the flow)
δ ( )	Dirac delta function
δ_1	displacement thickness
$\Delta\omega$	frequency bandwidth
η, η_2, $\eta_{i\pm1}$	loss factor for the panel
η_{21}, $\eta_1^{i\pm1}$	coupling loss factor

LIST OF SYMBOLS (continued)

θ	average eddy lifetime
κ	radius of gyration
$\underset{\sim}{\lambda}$	separation $(x-x^1)$
λ_p	flexural wavelength of panel
ν	kinematic viscosity
Π	power input per unit area of the panel
Π_{HC}	power input per unit area of the panel in the hydrodynamically coincident regime
Π_{HS}	power input per unit area of the panel in the hydrodynamically slow regime
Π_m	measured power accepted by panel
Π_{th}	theoretical power accepted by panel
ρ	fluid density
ρ_p	density of panel material
ρ_s	surface mass density
τ	time delay $t-t^1$
ϕ	angle between k and k_1 axis
ϕ_c	Mach angle for free bending waves
ω	response radian frequency
ω^1	frequency variable
ω_h	hydrodynamic critical radian frequency

PART I. STUDIES OF STRUCTURAL RESPONSE

1. ESTIMATION OF BOUNDARY LAYER POWER INPUT TO A STRUCTURE

The take-off and launch phases of aircraft and spacecraft produce very severe acoustic environments for the structure, personnel, and equipments. The need for accurate data on the response and fatigue (or malfunction) of these vehicles has led engineers to the construction of elaborate and costly facilities for the simulation of intense acoustic environments. A well-known example is the Sonic Fatigue Facility of the Research and Technology Division, Wright-Patterson Air Force Base, Ohio.

In the flight regimes of these vehicles that are associated with a large dynamic head q, excitation by the turbulent boundary layer can become a very important source of skin vibration and interior noise. Some of the Mercury flights, for example, showed that the noise and vibration levels during the "max q" period significantly exceeded those experienced during the launch phase (Ref. 1). The magnitude and importance of these environmental loads naturally leads one to inquire whether an acoustic facility can be used to simulate these loads or their effects.

The simulation of turbulent boundary-layer loads ideally would mean the reproduction of the distribution of acoustic pressures over the vehicle, with correlation and convection properties very similar to those of the turbulence. In a sound field the speed of propagation, the wavelength, and the frequency are related. This is not the case for the turbulent field, where a particular wavelength component may have a whole distribution of frequencies and/or convection speeds (Ref. 2).

If one is concerned primarily with vibratory response, then it is the turbulent energy at wavelengths near the free bending wavelength in the panel which account for most of the excitation (Ref. 3). Even if the simulation is restricted to this small group of wavenumbers near the bending wavenumber, the simulation of loads still is not possible, since the acoustic frequencies corresponding to such wavelengths generally would be higher than the frequencies of panel response.

These difficulties may be avoided if one does not insist upon reproducing the spatial and temporal details of the pressure field. When the system is sufficiently reverberant, the details of the source are unimportant if one uses a source

distributed over a large area. For such a system the reverberant energy dominates the input energy in any small region of the system. This condition holds for most conventional aerospace structures. The response of the structure is determined by the circulating energy and not by the method used to get the energy into the system.

The resonant response of a panel is also somewhat insensitive to the source of mechanical excitation. This response depends primarily on the mechanical power supplied to the panel by the environment, regardless of details of coupling. It also depends on the structural damping. In order to simulate the service environment-structural system, we must be able to calculate the expected mechanical power absorbed by the structure.

In part II, we propose to simulate the structure and its damping by using a test arrangement that is characteristic of the types of service structures to be encountered. The source of mechanical power can be any source of energy available in the facility which will simulate the desired frequency spectrum and approximate the spatial distribution. The excitation chosen for study here will be a series of "wall-jets". This system can be actuated by the main air supply in the facility. In part I of this report, we concentrate on the mechanical power supplied to panels by a boundary layer and by wall-jet flows.

1.1 Response of a Simple Panel to Boundary-Layer Noise

The vibratory response of the modes of a simply supported thin panel to convected turbulence was computed by Dyer (Ref. 4). He distinguished three primary categories of modal behavior; when the trace wavespeed of the mode at resonance projected along the direction of convection is

(a) less than the convection speed, the modes are called hydrodynamically slow (HS).

(b) equal to the convection speed the modes are called hydrodynamically coincident (HC).

(c) greater than the convection speed the modes are called hydrodynamically fast (HF).

These regimes are readily displayed in wavenumber space as shown in Fig. 1. The trace wavespeed in the direction of convection is $c_B/\cos\phi$, and the locus of modes for which $c_B/\cos\phi = U_c$ is the "HC mode" semicircle of radius $U_c/2\kappa c_\ell$. The HS modes fall within this circle, the HF modes without.

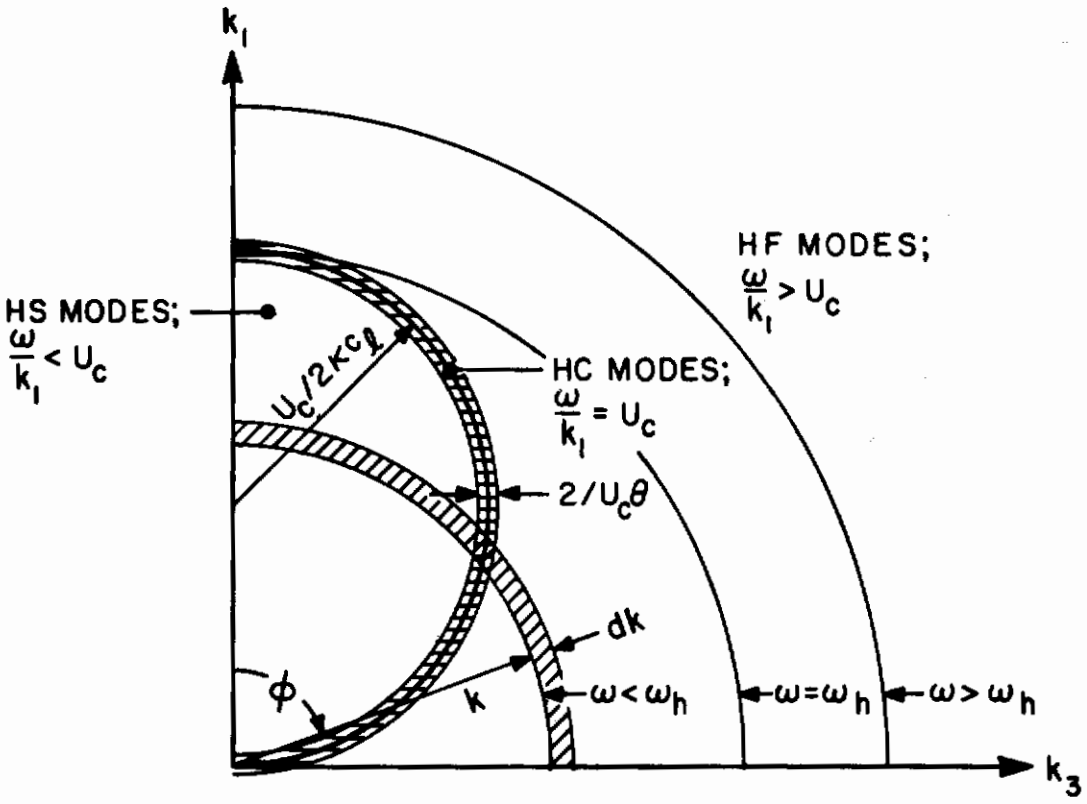

FIG. 1 PLOT OF WAVE NUMBERS, PATTERN IN k-SPACE

1.1.1 Low-speed convection, $U_c \ll c_B$

Dyer's model of the pressure correlation pattern was

$$\overline{p(\underline{x},t)p(\underline{x}'_1,t')} = p_h^2 A_t \, \delta\{x_1 - x'_1 - U_c(t-t')\} \, \delta(x_3 - x'_3) \, e^{-|t-t'|/\theta}, \tag{1.1}$$

where p_h is the turbulent rms pressure, U_c is the convection speed, A_t is a correlation area, and θ is an average eddy lifetime. The spatial correlation in the moving frame, $x_1 = U_c t$, is assumed to be very small and the time correlation is a simple exponential. When $U_c \ll c_B$, the HC locus in Fig. 1 collapses to the origin and the response is composed entirely of HF modes. By grouping the modes in frequency bands, one can compute the spectral density of panel response velocity. The result is (Ref. 5).

$$\mathcal{Y}(\omega) = p_h^2 G_\infty \, A_t \mathcal{P}_\tau(\omega)/\omega\eta\rho_s \, , \tag{1.2}$$

where $G_\infty = (8\rho_s \kappa c_\ell)^{-1}$ is the mechanical point input conductance of an infinite flat plate. The loss factor for the panel is η, and ρ_s is the surface mass density. In Eq. (1.1) the moving axis frequency spectrum is

$$\mathcal{P}_\tau(\omega) = \frac{\theta}{\pi} (1 + \omega^2 \theta^2)^{-1} \tag{1.3}$$

although this precise form is not required for the validity of Eq. (1.2) The form of $\mathcal{P}_\tau(\omega)$ is shown in Fig. 2, there generally being fairly uniform energy content up to a frequency $\omega = 1/\theta$, beyond which the energy diminishes rapidly.

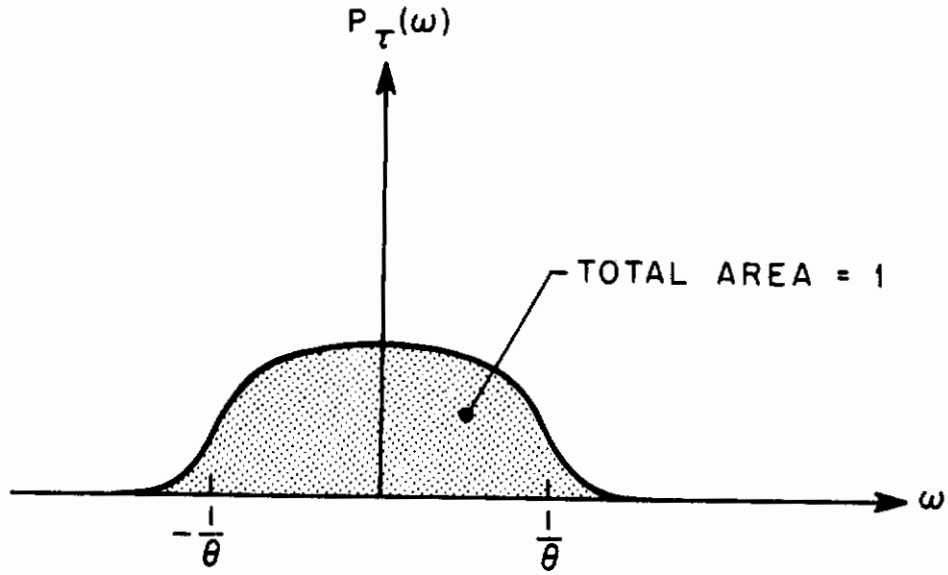

FIG. 2 GENERAL FORM OF MOVING AXIS TEMPORAL POWER SPECTRUM

The equivalent "correlation area" A_t is determined by the strength of the wavenumber spectrum at the free bending wavenumber for the plate. It is (Ref. 6)

$$A_t \equiv 4\pi^2 \left\langle \Phi_{\underset{\sim}{\chi}}(\; |\underset{\sim}{\kappa}| = \kappa_p \; , \phi \;) \right\rangle_\phi \qquad (1.4)$$

where $\Phi_{\underset{\sim}{\chi}}|\underset{\sim}{\kappa}|$ is normalized to unity. The form of A_t for low-speed (incompressible) turbulence is given in Fig. 3 (Ref. 7). The excitation is seen to be most effective in the range where the bending wavelength is the reciprocal of the displacement thickness, and drops off above and below this value. We note from (1.2) that the frequency spectrum $\Phi_\tau(\omega)$ is directly reflected in the response spectral density.

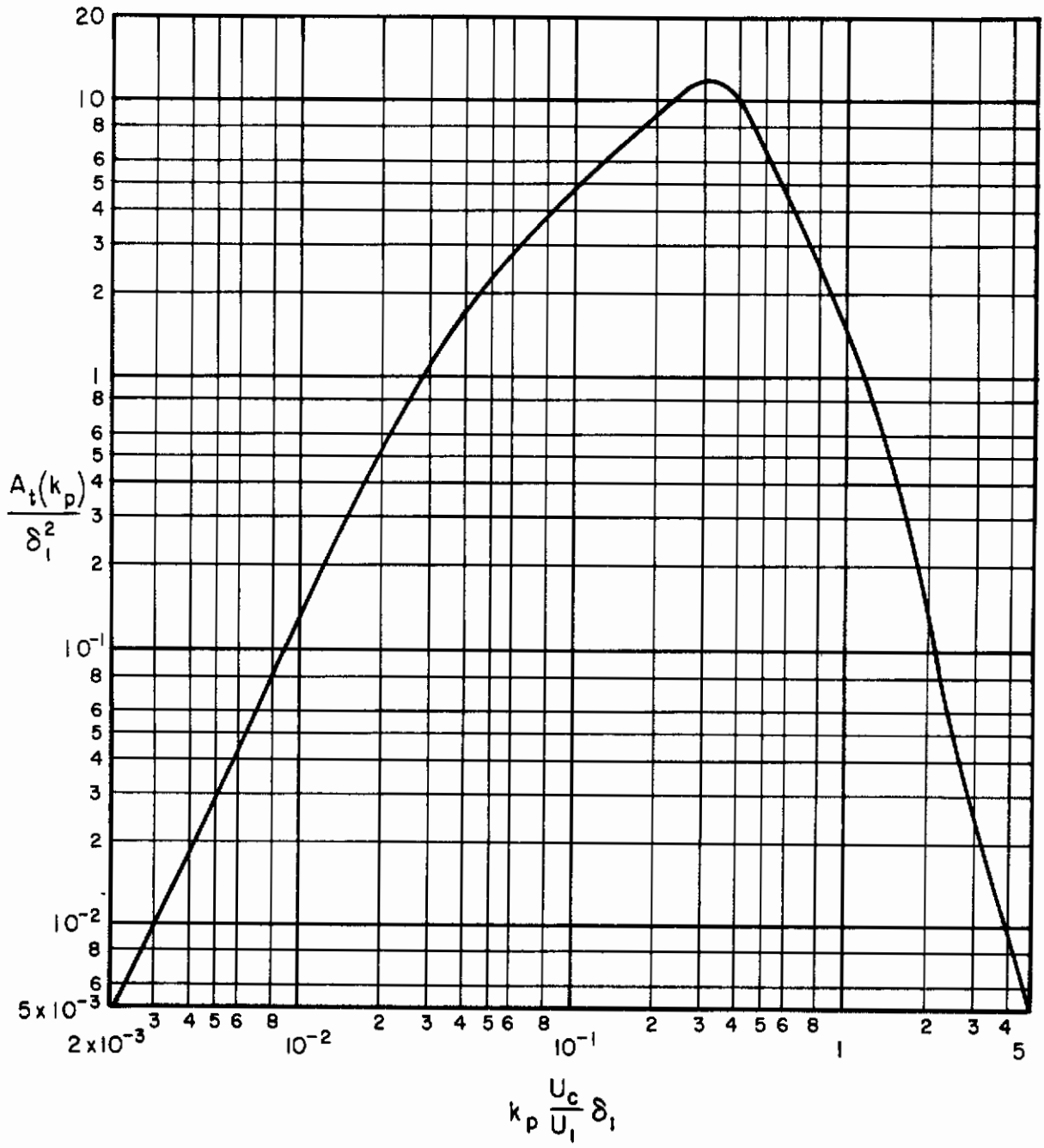

FIG. 3 THE EQUIVALENT CORRELATION AREA $A_t(k_p)$ AS A FUNCTION OF PLATE WAVE NUMBER FOR A GLIDER WING

1.1.2 High-speed convections, $U_c > c_B$

When the convection speed exceeds the trace wavespeed, which is the situation depicted in Fig. 1, Dyer's results may again be applied. In this instance, however, it is useful to compute the power input to an infinite panel, since the calculations are simpler to perform and lead to the same results after averaging over groups of modes.

For the infinite panel, one begins with the equation of motion

$$\kappa^2 c_\ell^2 \nabla^4 y + \frac{\partial^2 y}{\partial t^2} + \omega\eta \frac{\partial y}{\partial t} = \frac{p}{\rho_s} \tag{1.5}$$

and expresses the displacement, y, and pressure, p, as Fourier integrals in time and space. The power input per unit area of the panel becomes (Ref. 8)

$$\Pi = - i p_h^2 \int \omega d\omega \int d\underset{\sim}{k} \frac{\mathcal{P}(\underset{\sim}{k},\omega')}{\rho_p h \kappa^2 c_\ell [\, k^4 - k_p^4(1+i\eta)]} \tag{1.6}$$

where $\mathcal{P}(k,\omega')$ is the spectral density of the turbulent pressure field in a frame moving at the convection speed. The frequency variable is $\omega' = \omega - k_1 U_c$ where ω is the response frequency and k_1 is the component of wavenumber in the direction of convection.

The spectrum $\mathcal{P}$ is the transform of the correlation function $\overline{pp'}$

$$p_h^2 \mathcal{P}(\underset{\sim}{k},\omega) = (2\pi)^{-3} \int d\underset{\sim}{\lambda}\, dt\, \overline{pp'} \exp(i\underset{\sim}{k}\cdot\underset{\sim}{\lambda} - i\omega t) \tag{1.7}$$

If the temporal and spatial correlations are assumed to separate in a convecting frame, then a similar separation will occur in the spectra:

$$p_h^2 \mathcal{P}_{\underset{\sim}{x}} (\underset{\sim}{k}) \mathcal{P}_\tau(\omega) = F \left\{ \tilde{\mathcal{P}}_{\underset{\sim}{x}} (\underset{\sim}{\lambda}) \tilde{\mathcal{P}}_\tau(t) \right\} \qquad (1.8)$$

If the pattern is uniformly convected, then the fixed-frame spectrum is related to the moving spectrum by

$$p_h^2 \mathcal{P}_{\underset{\sim}{x}} (\underset{\sim}{k}) \mathcal{P}_\tau (\omega - k_1 U_c) = F \left\{ \tilde{\mathcal{P}}_{\underset{\sim}{x}} (\lambda_1 - U_c\tau, \lambda_3) \tilde{\mathcal{P}}_\tau(\tau) \right\} , \qquad (1.9)$$

as above.

When the convection is slow, as on the hull of a ship or on an aircraft at take-off speeds, then $k_1 U_c \ll \omega$ and the wavenumber and frequency integrations in Eq. (1.6) separate. The resulting power input is equated to the dissipation $\omega \eta \rho_s \mathcal{U}(\omega)$, and the velocity spectrum given in Eq. (1.2) results. Thus, the infinite-plate and finite-panel results are consistent at low speeds, and we may expect them to be consistent at high speeds as well.

The wavenumber pattern for the infinite plate is depicted in Fig. 4. It is similar to Fig. 1 except that now wave components in the plate can be related directly with any point on the diagram. Instead of modes, there is now a breakdown into HS, HC, and HF waves. From the analysis, it turns out that the largest response (or power input to the plate) occurs at the intersection of the $k = k_p$ circle and the HC wave locus. For these waves, the temporal decay of the turbulence is unimportant, its wavenumber spectrum determining the response at $k = k_p$ and consequently at frequency $\omega = k_p^2 \kappa c_\ell$. The formal result is (Ref. 8)

$$\Pi_{HC} = 4\pi p_h^2 G_\infty \mathcal{P}_{\underset{\sim}{x}}(k = k_p, \phi_c)/k_p U_c \sin \phi_c , \qquad (1.10)$$

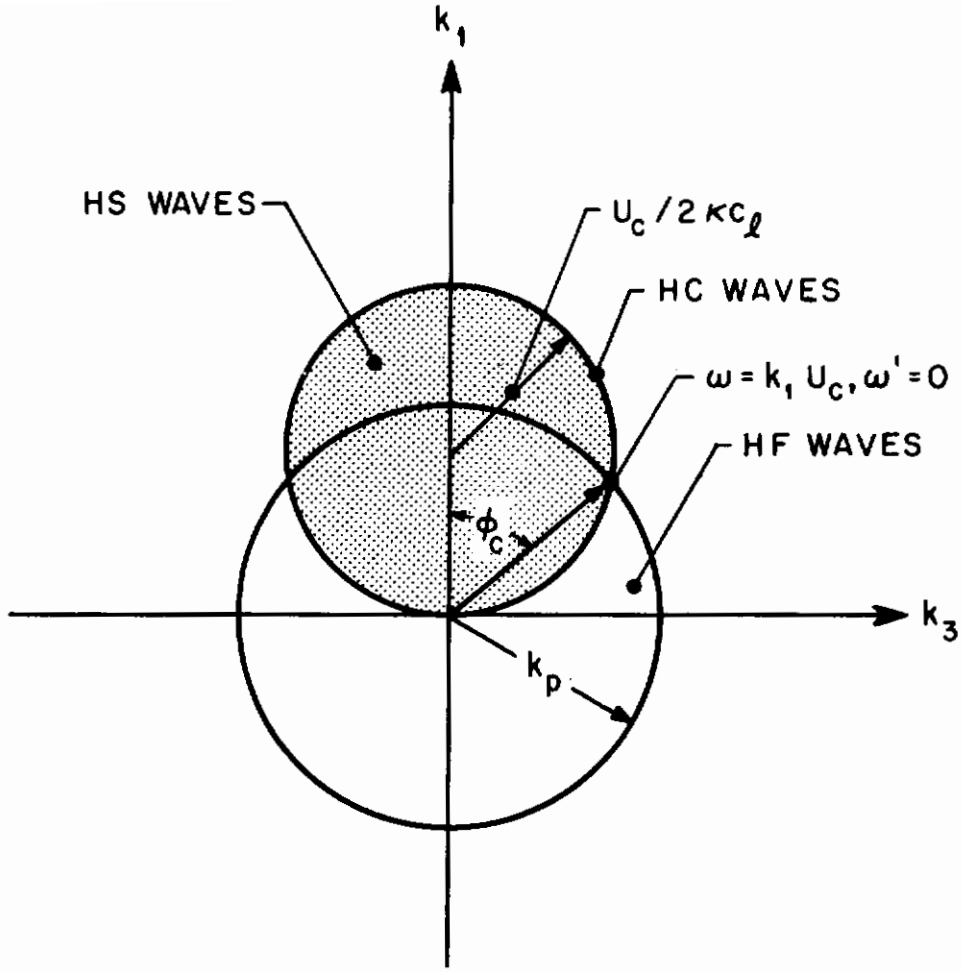

FIG.4 LOCI OF CONSTANT FREQUENCY AND HYDRODYNAMIC COINCIDENCE IN k PLANE

which may be converted to a velocity spectrum by equating input and dissipated power, as above. The primary feature of this result is the absence of $\mathcal{P}_T(\omega)$. In simulating the power input from high-speed turbulence, therefore, one is concerned primarily with simulating a wavenumber spectrum. This spectrum is quite smooth, having roughly a 10-dB variation over 1.5 decades in wavenumber or 3 decades in frequency, as seen by reference to Fig. 5.

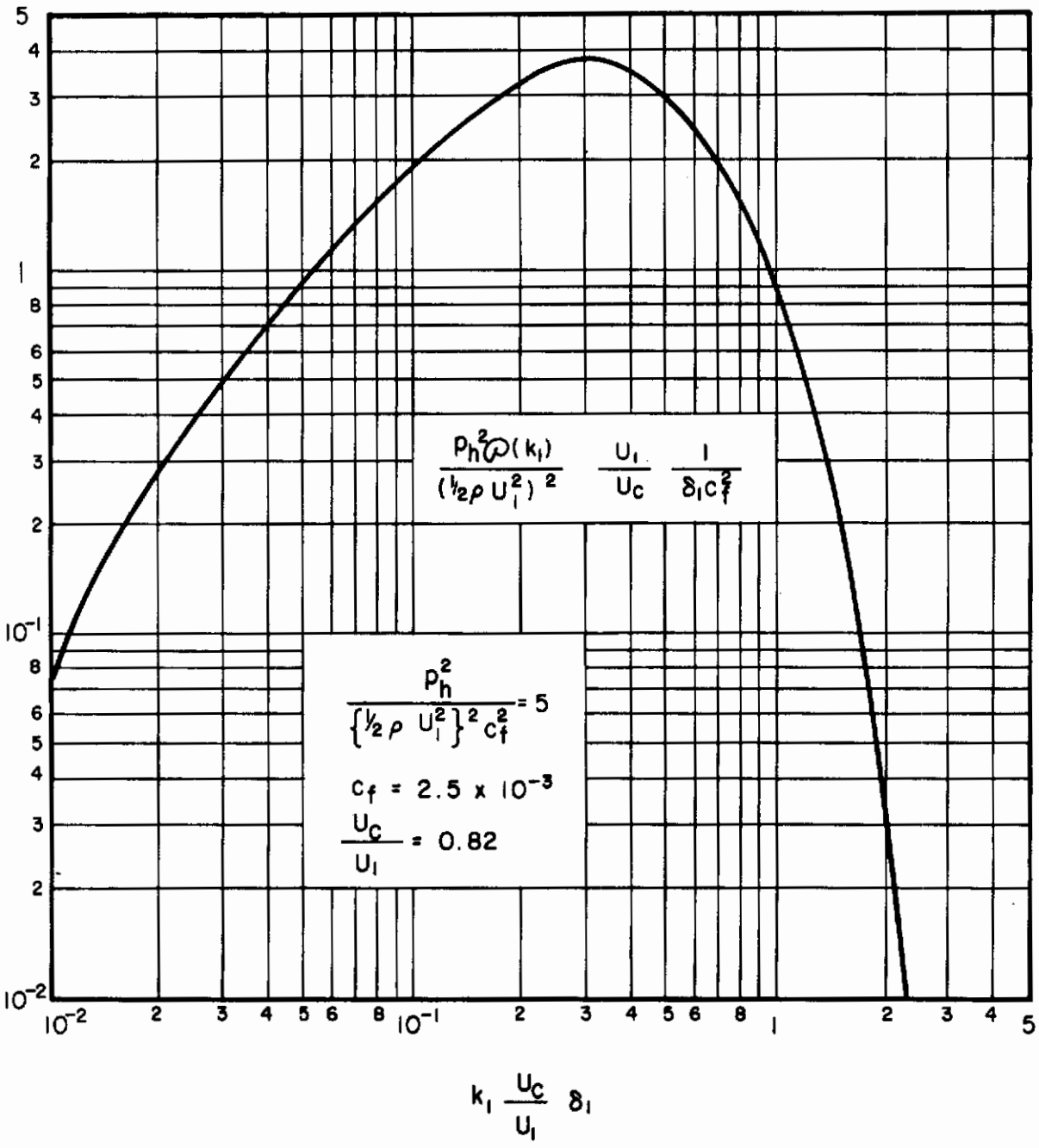

FIG. 5 THE ONE-DIMENSIONAL WAVE NUMBER SPECTRAL FUNCTION $\Phi(k_1)$ CALCULATED USING TAYLOR'S HYPOTHESIS, FROM HODGSON'S EXPERIMENTAL RESULTS FOR A GLIDER WING

At very high convection speeds or very low frequencies, there is another change in form of excitation. This is because the HC locus shown in Figs. 1 and 4 becomes nearly coincident with the $k_1 = 0$ axis. If we put $k_1 = 0$ in Eq. (1.9) we again have $\omega' \simeq \omega$ and we revert to the form of the HF results for low-speed excitation. In addition, at low frequencies the modal structure of the panel response discriminates against HC response. The frequency range where these effects become important is discussed in the following section.

1.2 Description of Flight Regimes for a Supersonic Transport

1.2.1 Boundary-Layer Parameters

The design objectives for the Supersonic Transport envisage designs for Mach 2 (aluminum) and Mach 3 (titanium). An approximate flight profile (Ref. 9) is given in the following table:

TABLE I

APPROXIMATE SST FLIGHT PROFILE

Mach Number	Altitude, ft	Air Speed, ft/sec U_1	Dynamic Pressure q, lbs/sq ft
1	30,000	1,000	430
1.5	46,000	1,500	490
2	50,000	2,000	700
2.5	54,000	2,500	930
3	60-70,000	3,000	770

The sound speed for the altitudes shown in the U. S. Standard Atmosphere range from 995 ft/sec at 30,000 ft to 968 ft/sec at 60,000 ft and 971 ft/sec at 70,000 ft. For the purposes of our estimates the sound speed can be taken as constant and approximately equal to 1,000 ft/sec. From this speed and the Mach number the approximate air speed is obtained, as shown in Table I. Using this air speed and air density, ρ, as given for the U. S. Standard Atmosphere (Ref. 10), the dynamic head q is determined from $q = 1/2\ \rho\ U_1^2$. This quantity will be needed later.

These air speeds correspond to the free-stream velocity. To estimate the effective convection velocity U_c on the surface of the aircraft, the results Kistler and Chen (Ref. 11) obtained in a supersonic wind tunnel can be used. According to this study, the ratio of convection speed U_c to free-stream speed U_1 (air speed) is 0.8 for $M \leq 1.5$, 0.7 for $M = 2$ and 0.6 for $M \geq 3$.

A second important parameter describing the turbulent boundary layer is the displacement thickness, δ_1, of the boundary layer. No direct measurements on high-speed vehicles are available, but estimates can be inferred from measurements of pressure fluctuation spectra on the Scout flight vehicle and Hodgson's measurements on a glider wing (Ref. 12). As δ_1 is expected to change only very slowly with Mach number, one can compare the peaks of Hodgson's generalized spectrum with experimental data obtained for various Mach numbers. Hodgson's spectrum peaks at a value of $\omega\delta_1/U_1 = 0.4$, when plotted in octave bands. Spectra measured on the Scout vehicle (Ref. 13) 72 feet from the nose have a peak in the 1200-2400 Hz band for $M \simeq 1.8$ and in the 2400-4800 Hz band for $M = 3.3$. This leads to estimates of δ_1 equal to about 0.07 ft. Since we are interested in the excitation of panels about 200 ft from the nose of the SST and since δ_1 is expected to grow at a rate roughly proportional to the distance, we arrive at an estimate of $\delta_1 \simeq 0.2$ ft for the SST.

Another estimate of δ_1 due to Schlichting (Ref. 14) is as follows:

$$\delta_1 \simeq 4.6\ 10^{-2}\ x\ (\nu/U_c x)^{1/5}\ , \qquad (1.11)$$

where x is the distance along the fuselage from the point of transition and ν is the kinematic viscosity. For M = 3 and x = 200 ft, $\delta_1 \simeq 0.07$ ft. The variation of displacement thickness with Mach number does become important for higher Mach numbers (Ref. 15). When M = 2, it is about twice the value given in Eq. (1.11). This corresponds more nearly to the value found in the previous paragraph for data on the Scout vehicle. In the following calculations, a value of $\delta_1 = 0.15$ ft (~2 inches) will be used.

A third important parameter describing the turbulent pressure field is the total mean-squared surface pressure fluctuation p_h^2. Except for buffeting loads in the transonic regime, flight tests on the Scout vehicle (Ref. 13) indicate that $\sqrt{p_h^2}/q = 0.006$, a value also obtained in other studies. Values of p_h are given in Table II.

TABLE II

ESTIMATED CONVECTION SPEED AND TBL PRESSURE FLUCTUATIONS FOR SST

M	U_c, ft/sec	RMS Pressure Fluctuations p_h, lbs/sq ft
1	800	2.6
1.5	1,200	3.0
2	1,400	4.2
2.5	1,800	5.6
3	2,100	4.6

1.2.2 Power Accepted by a Panel in the Hydrodynamically Coincident Regime

It is well known that the response of a plate to convected turbulent pressure fluctuations depends on a comparison of the convection speed with the trace speed of the bending waves in the direction of the convection speed. The case of hydrodynamic coincidence is important since it results in large response. We wish to estimate the power accepted by the structure in this case, i.e., where the trace speed of the free bending waves in the structure along the direction of convection (1-axis) equals U_c. The points in the k_1-k_3 wavenumber plane in this regime (for variable ω) are on a circle of radius $U_c/2\kappa c_\ell$ (Ref. 16) with center at $k_1 = U_c/2\kappa c_\ell$, $k_3 = 0$. The hydrodynamic coincidence frequency is defined by $\omega/k_1 = \omega_h/k_p = U_c$ where k_p is the wavenumber of the free bending waves. Since $k_p = (\omega/\kappa c_\ell)^{1/2}$, one finds $2\pi f_h = \omega_h = U_c^2 \kappa c_\ell$.

For the structures and convection speeds of interest here, f_h lies between about 5 and 40 kHz. One usually is interested in lower frequencies, e.g., the region of resonant modes of finite structures and of interference with speech and hearing. There $\omega << \omega_h$ and excitation is dominant for bending waves traveling at the "Mach angle" ϕ_c with respect to the direction of turbulence convection. Moreover, $\cos \phi_c = (\omega/\omega_h)^{1/2}$. For $\omega = 10^{-2}\ \omega_h$, $\phi_c \simeq 84^0$, and the bending waves travel in a direction essentially perpendicular to the direction in which the turbulence is convected.

The wavenumbers of the resonant modes of a finite panel form a rectangular grid in the k_1-k_3 plane at a pitch of π/L_1 and π/L_3, where L_1 and L_3 are the linear dimensions of the panel. It is of interest to calculate the frequency $f_{h\ell}$ at which the line π/L_1 parallel to the k_3 axis and the coincidence semicircle intersect. This is the approximate lower-frequency limit to the HC excitation and is given by $f_{h\ell} \simeq U_c/2L_1$, as can be seen from Fig. 6. For $L_1 = 2$ ft, $f_{h\ell}$ ranges from about 250 Hz to 700 Hz for the range of U_c considered. Note that, as U_c increases, $f_{h\ell}$ increases in direct proportion, whereas f_h increases in proportion to U_c^2.

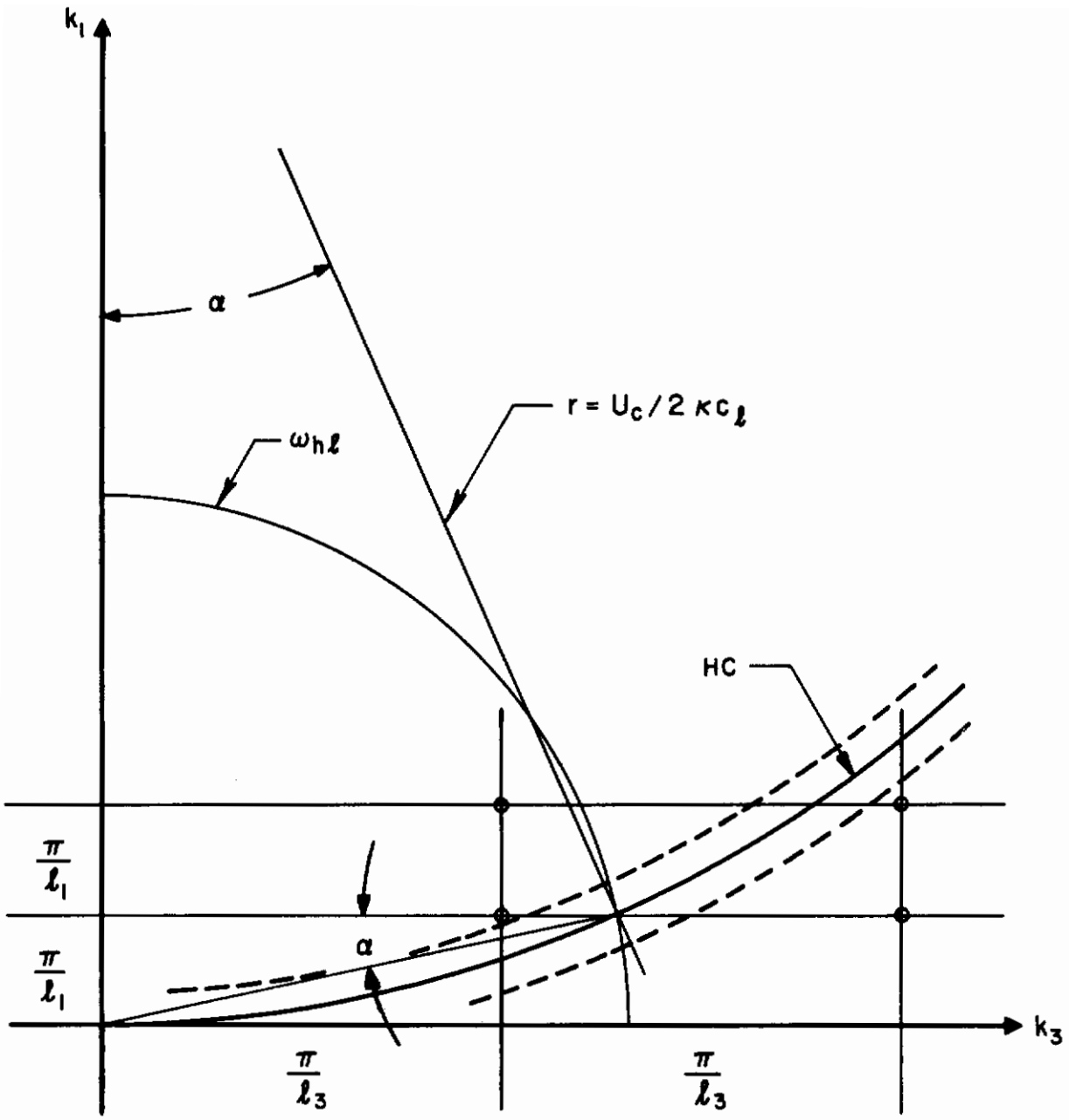

FIG. 6 CALCULATION OF THE LOWER FREQUENCY LIMIT TO THE HYDRODYNAMICALLY COINCIDENT EXCITATION

Lyon (Ref. 17) has shown that most of the energy input is into bending waves near the Mach angle, ϕ_c, when the wavelength along the k_3 axis is less than about $10^3\delta_1$, or 150 ft in the present case. This is readily achieved for the structures of interest here for frequencies above $f_{h\ell}$ (see below). The power per unit area, Π_{HC}, accepted by the panel in the regime of hydrodynamically coincident response in a frequency band $\Delta\omega$ has been also calculated (Ref.17):

$$\Pi_{HC} = p_h^2 \frac{G_\infty A_t(k_p\delta_1)}{k_p U_c \sin\phi_c} \Delta\omega \qquad (1.12)$$

where $G_\infty = (8\rho_p h\kappa c_\ell)^{-1}$ is the transverse point conductance of an infinite panel of density ρ_p and thickness h. $A_t(k_p\delta_1)$ is the effective correlation area shown in Fig. 3 (Ref. 18). For third-octave bands, $\Delta\omega/\omega \simeq 1/4$ and $(\omega/k_p U_c) = \cos\phi_c$. Hence, in one-third octave bands,

$$\Pi_{HC}(1/3\ OB) = \frac{p_h^2 G_\infty}{2\pi} A_t(k_p\delta_1) \cot\phi_c \qquad (1.13)$$

1.2.3 Power Accepted by a Panel in the Hydrodynamically Slow Regime

In this regime, the trace speed of the free bending waves in the structure along the direction of convection is less than U_c. For variable ω, the points in the k_1-k_3 wavenumber plane now lie within the circle $\{k_1-(U_c/2\kappa c_\ell)\}^2 + k_3^2 = (U_c/2\kappa c_\ell)^2$, and $f = \frac{\omega}{2\pi}$ is less than $f_{h\ell}$, the lower limit for the hydrodynamically coincident regime.

The power per unit area accepted by the panel in the hydrodynamically slow regime, Π_{HS}, in one-third octave bands, is given as

$$\Pi_{HS}(1/3\ OB) = p_h^2 G_\infty \frac{A_t(k_p\delta_1)}{\pi} \frac{\omega\theta}{1+\omega^2\theta^2}, \qquad (1.14)$$

where θ is a time constant equal to $25\delta_1/U_c$ and G_∞, $A_t(k_p\delta_1)$ and p_h^2 are the same parameters used for the hydrodynamically fast regime.

1.2.4 Calculation of Power per Unit Area for a Titanium Panel

A representative panel structure of the fuselage of the SST might consist of a titanium alloy skin 0.050 in. thick, mounted between ring frames about 1-1/2 ft apart, and stiffened by longitudinal strips. We estimate $\rho_p \simeq 1.6 \times 10^{-1}$ lbs/in.^{3} and $c_\ell \simeq 1.6 \times 10^4$ ft/sec. The radius of gyration κ of the cross section is $\kappa = h/\sqrt{12} = 1.2 \times 10^{-3}$ ft, and $\kappa c_\ell \simeq 20$ ft^2/sec. The transverse point conductance for this structure has the value $G_\infty \simeq 1.8 \times 10^{-1}$ ft/sec lb. The hydrodynamic frequency, f_h, and the lower frequency limit for HC excitation, $f_{h\ell}$, are calculated for each value of M and are given in Table III. The time constant θ for the TBL is also given in Table III.

TABLE III

FREQUENCY LIMITS FOR A TITANIUM PANEL AND TBL TIME CONSTANT

M	$f_{h\ell}$(Hz)	f_h(Hz)	θ (msec)
1.0	270	5300	4.7
1.5	400	12000	3.1
2.0	470	16000	2.7
2.5	600	27000	2.1
3.0	700	36000	1.8

The effective correlation area $A_t(k_p\delta_1)$, is determined from Fig. 3 for frequencies from 63 Hz to f_h. Figure 3 gives values of $A_t(k_p\delta_1)$ only for $k_p \frac{U_c}{U_1} \delta_1$ up to 5, so that Π_{HC} was calculated for f up to f_h only for the case where M=1. The change in slope which occurs for the M=1 for f near f_h probably would occur for cases where $M > 1$, had the power been calculated for the region where f is nearly f_h.

Π_{HC} now is calculated for $f_{h\ell} < f < f_h$, and Π_{HS} is calculated for 50 Hz $< f < f_{h\ell}$. The results are shown in Fig. 7, where Π_{HS} and Π_{HC} are given in dB re 10^{-12} watt vs frequency in one-third octave bands.

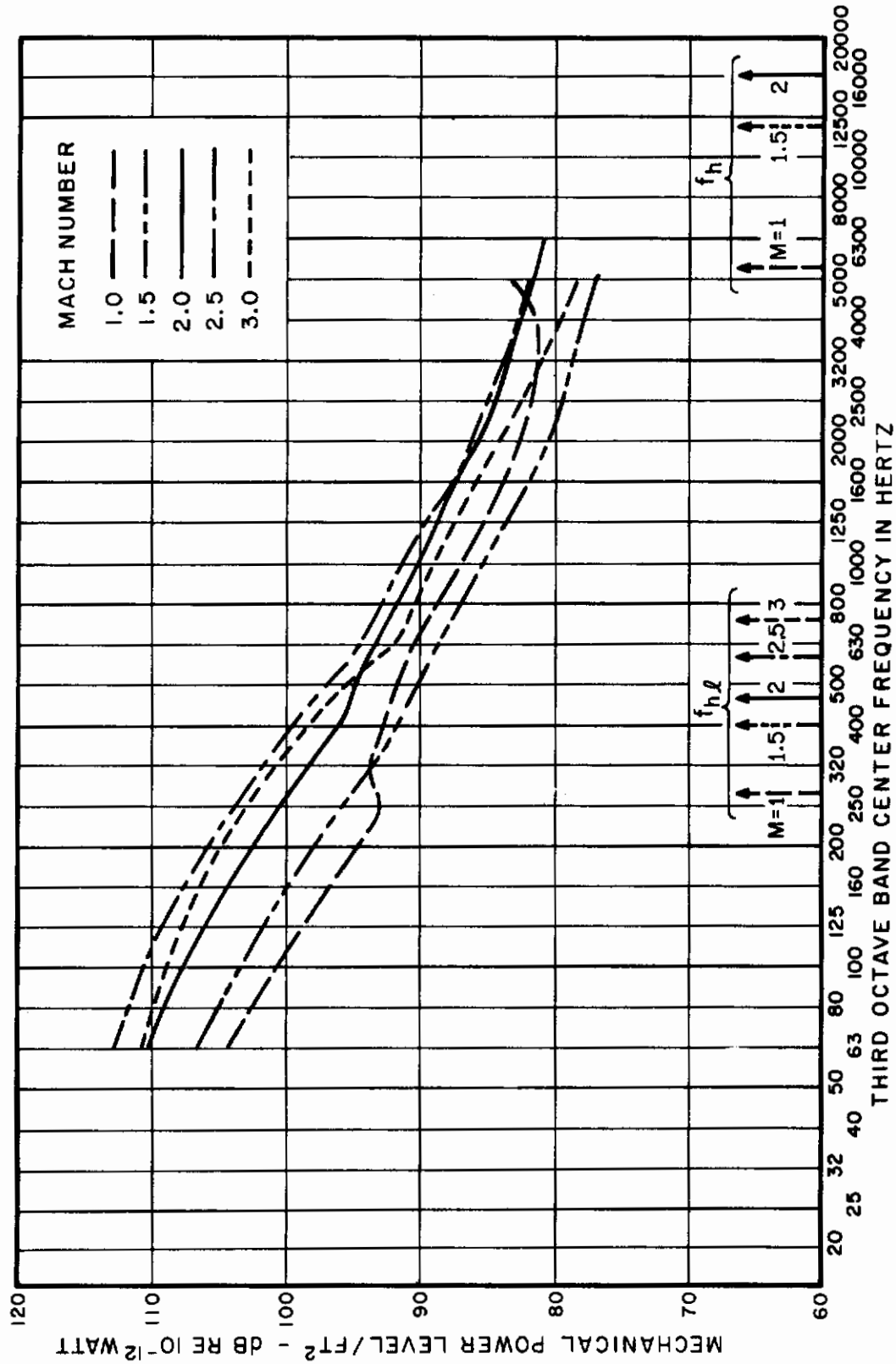

FIG. 7 POWER ACCEPTED BY TITANIUM PANEL IN HYDRODYNAMICALLY SLOW AND COINCIDENT REGIMES FOR VARIOUS MACH NUMBERS

2. EXCITATION OF FLEXIBLE PANELS BY A WALL-JET

2.1 Introduction

The use of turbulent jets to excite structures offers a possibility for injecting broadband mechanical power over a localized region of a structure with very simple equipment. The availability of sizeable amounts of airflow in the Wright Field Acoustic Test Facility makes the use of such jets unusually attractive.

We shall consider the excitation of a flat panel by a turbulent "wall-jet." A wall-jet is obtained by placing a nozzle close to and perpendicular to a panel, as shown in Fig. 8. The fluid dynamic theory of such a jet has been studied by Glauert (Ref. 19), and its turbulent velocity and pressure fields have been examined by Hodgson (Ref. 20). It is particularly this latter work that will be of help to us in our considerations here.

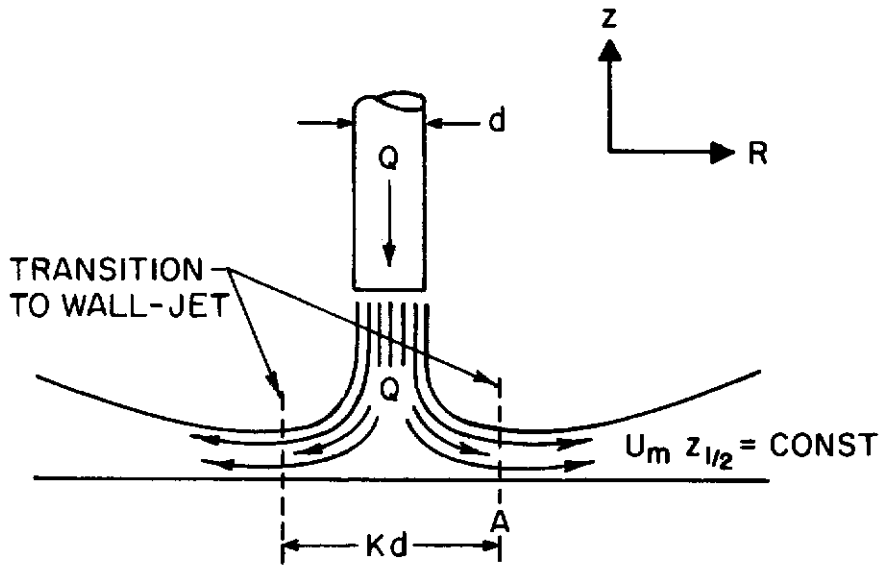

FIG. 8 FLOW PATTERN FOR NORMALLY IMPINGING JET AND TRANSITION TO WALL-JET

Our approach to the problem will be quite elementary. We shall make a simple equivalence between the fluctuating pressure field of the wall-jet and a point mechanical excitation, in a manner similar to the calculation made for boundary-layer turbulence (Ref. 21).

2.2 Fluid Dynamics and Turbulent Properties of the Radial Wall-Jet

At radial distance R from the jet axis, the mean flow from the nozzle shown in Fig. 8 has the mean velocity profile given in Fig. 9. The velocity maximum is U_m and the distance to the half-velocity point in the jet regime of the flow is $z_{1/2}$. Glauert's analysis indicated that the dependence of these quantities on distance was

$$U_m \propto R^{-1.096} \quad , \quad z_{1/2} \propto R^{1.01} \tag{2.1}$$

while Hodgson's experimental results gave

$$U_m \propto R^{-1.0} \quad , \quad z_{1/2} \propto R^{0.94} \tag{2.2}$$

For the purposes of our discussion, we shall assume

$$U_m \propto R^{-1} \quad , \quad z_{1/2} \propto R \ . \tag{2.3}$$

In his studies of the turbulent pressure field of the radial wall-jet, Hodgson found that the correlation scales vary directly with $z_{1/2}$. The fixed microphone frequency spectrum is shown in Fig. 10. The measured transverse (azimuthal) correlation function was very close to the functional form $\exp(-|\lambda|/\ell_3)$ where $\ell_3 \simeq 1.6 z_{1/2}$ (Ref. 22) which has a wavenumber spectrum

$$\mathcal{P}_3(k_3) = \frac{\ell_3}{\pi} (1 + k_3^2 \ell_3^2)^{-1} \tag{2.4}$$

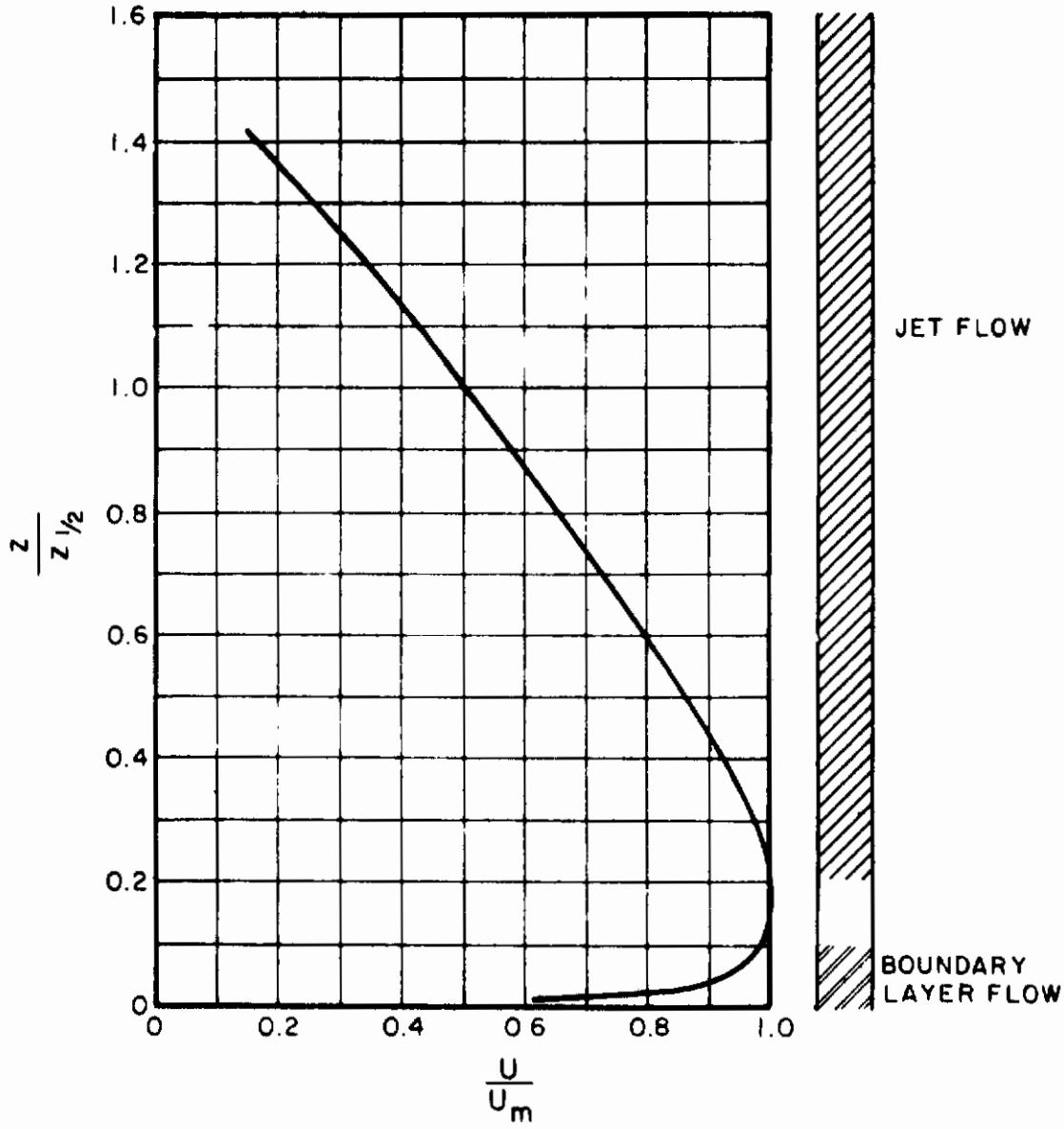

FIG. 9 MEAN VELOCITY PROFILE OF RADIAL WALL-JET

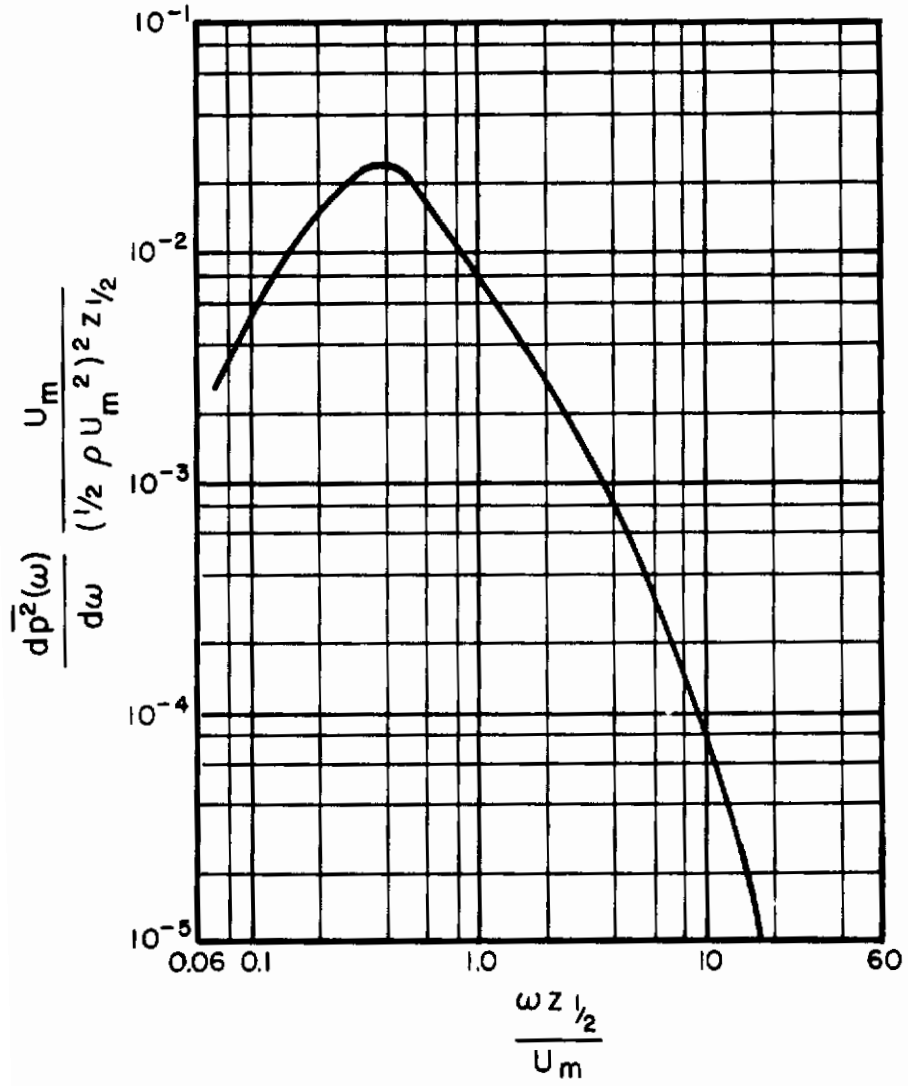

FIG 10 WAVE NUMBER SPECTRUM AS MEASURED BY FIXED MICROPHONE

The inference from this is that we can define an effective turbulence correlation area by

$$A_t = A_{t(1)} \frac{R^2}{R_1^2} \tag{2.5}$$

where $A_{t(1)}$ is the correlation area at a distance R_1 from the jet axis.

As the turbulent eddies move, they decay because of nonlinear mixing processes and viscous dissipation. Since the eddy scale is increasing with R and the convection velocity is decreasing, this decay time will tend to increase. Hodgson's experiments suggest that the proper relation for the local temporal scale is

$$\theta = 5z_{1/2}/U_m \propto R^2 \ . \tag{2.6}$$

This may be compared with $\theta \simeq 25\delta_1/U_c$ for the case of boundary-layer turbulence.

2.3 Simplified Calculation of Fluctuating Force Exerted by Wall-Jet on Rigid Plane

The equivalence between a wall-jet and a mechanical shaker, which applies a certain rms force to a panel in frequency bands, can be computed. We do this by considering the number of uncorrelated eddies, dN, which are included in an interval dR (see Fig. 11). If the correlation area of the turbulence is A_t, then

$$dN = \frac{2\pi R}{A_t} \, dR. \tag{2.7}$$

Each coherent element produces a mean square force

$$\overline{df^2} = p_h^2 \, A_t^2 \, \mathcal{P}_\tau(\omega) \, d\omega \, dN \tag{2.8}$$

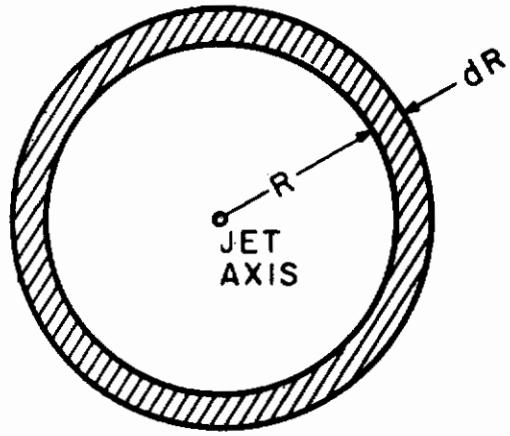

FIG. II AREA ELEMENT IN CALCULATION OF EQUIVALENT FORCE

in the frequency interval $d\omega$. Here $\mathcal{P}_\tau(\omega)$ is the moving axis frequency spectrum, which, if we assume an exponential correlation function in convected coordinates, is given by

$$\mathcal{P}_\tau(\omega) = \frac{2\theta/\pi}{1+\omega^2\theta^2} \qquad (\omega > 0). \tag{2.9}$$

For our purposes it is not necessary to specify a particular form of this spectrum except to require "similarity" in the time scale:

$$\mathcal{P}_\tau(\omega) = \theta H(\omega\theta) \ . \tag{2.10}$$

The mean-square pressure was found by Hodgson to be

$$p_h^2 \simeq 4.5 \times 10^{-3}\ \rho^2 U_m^4 \propto R^{-4} \qquad (2.11)$$

If we normalize the variables in (2.8) to their observed values at a position $R = R_1$, we have

$$\overline{df^2} = p_{h(1)}^2 \frac{R_1^4}{R^4} A_{t(1)} \frac{R^2}{R_1^2} \theta H(\omega\theta)\, 2\pi R\, dR\, d\omega .$$

Since $\theta \propto R^2$, we can define

$$\omega\theta \equiv k_d^2 R^2 \qquad (2.12)$$

or, $\theta = k_d^2 R^2/\omega$. We next integrate over R to obtain all contributions to the excitation in a frequency interval $d\omega$:

$$F(\omega)d\omega = \int_{R=0}^{R=\infty} \overline{df^2} = \pi p_{h(1)}^2 A_{t(1)} R_1^2 \frac{d\omega}{\omega} \int_0^\infty 2k_d^2 R\, H(k_d^2 R^2) dR.$$

By its normalization, the integral over H has the value unity. Therefore

$$F(\omega) = \pi\, p_{h(1)}^2 A_{t(1)} R_1^2 \omega^{-1} . \qquad (2.13)$$

It is of interest to note that the time constant θ drops out of this calculation.

Once we can assign a value to the correlation area, A_t, the computation of the spectral density of the exciting power becomes simply a matter of measuring the mean flow profile of the wall-jet at some arbitrary radius R_1.

2.4 Theoretical Power Supplied to the Panel

On the basis of the simple equivalence we have drawn between the wall-jet excitation and a point mechanical excitation of the panel, the power accepted by the panel from a wall-jet is given by the relation

$$\Pi_{th} = F(\omega)\, d\omega\, G_\infty \tag{2.14}$$

where $F(\omega)$ is the spectral density of the exciting power in the turbulent wall-jet as given by Eq. (2.13), and G_∞ is the input conductance of an infinite panel, given by

$$G_\infty = \left(\frac{4}{\sqrt{3}}\ \rho_p\ c_\ell\ h^2 \right)^{-1} \tag{2.15}$$

where ρ_p is the panel density, c_ℓ the longitudinal wave velocity and h the panel thickness. The same equation applies to the impedance of a finite panel averaged over several modes. Our assumption is that, in the third-octave bands used in this experimental study, several modes of the panel will be excited. It should be noted that Eq. (2.14) implies a flat frequency spectrum of the input power to the panel when this is measured in third-octave bands or in any constant-percentage bandwidths.

2.5 Modifications to the Simple Theory

In developing the expression for the power spectral density contained in Eq. (2.13) we have, perhaps, oversimplified the problem. Although the simple analysis may provide an indication of the level of excitation to be expected from the wall-jet, it cannot describe the form of the frequency spectrum observed in the experimental phase of this study.

The power accepted from the turbulent flow by the test panel, in third-octave bands, may be written more generally as

$$\Pi = p_{h(1)}^2 \, R_1^4 k_d^2 G_\infty \int_{r_1}^{r_2} \frac{A_t}{(1 + k_d^4 R^4)} \frac{dR}{R} \qquad (2.16)$$

where G_∞ is as given in Eq. (2.15). Here we have made no assumptions regarding the dependence of A_t upon the system parameters. Also, we have replaced the limits of integration by the actual finite limits of the minimum jet radius ($R = r_1$) and the equivalent outer radius of the test panel ($R = r_2$).

2.5.1 Effect of Finite Plate and Jet Size

If we continue with the simple assumption that the correlation area is as given by Eq. (2.5) and consider only the effect of finite plate and nozzle dimensions upon the power accepted by the panel, Eq. (2.16) now becomes

$$\Pi = \frac{1}{2} p_{h(1)}^2 \, R_1^2 A_{t(1)} G_\infty \left\{ \text{Arctan} \left[\omega\theta_1 \left(\frac{r_2}{R_1} \right)^2 \right] - \text{Arctan} \left[\omega\theta_1 \left(\frac{r_1}{R_1} \right)^2 \right] \right\} \qquad (2.17)$$

where $\theta_1 = 5z_{1/2}/U_m$ is the time constant of the turbulence as measured at R_1. This expression now shows that the power accepted by the panel is frequency-dependent. The dependence, however, is too weak to account for the spectrum shape observed in some of the experimental studies to be described. When r_2 and r_1 tend towards infinity and zero, respectively, the expression for power reverts to that obtained by the earlier simple analysis.

2.5.2 Effect of Frequency-Dependence of Correlation Area

Perhaps the most serious shortcoming of the simple analysis is the assumption derived from Eqs. (2.3) and (2.5), that A_t is simply related to $z_{1/2}^2$, and is not frequency-dependent. A more realistic expression for the correlation area can be obtained by combining the expression for the transverse wavenumber spectrum given in Eq. (2.4) with the fixed-microphone frequency spectrum shown in Fig. 10. The resultant "equivalent" correlation area is normalized in terms of the plate wavenumber. Such a process has been carried out elsewhere by Ffowcs-Williams and Lyon (Ref. 5),using Hodgson's measurements on a glider wing. Their results are shown in Fig. 3. Since we are interested only in assessing the frequency-shaping effects of the more complicated expression for correlation area, let us assume their result to approximate the wavenumber dependence of A_t for the wall-jet.

The curve of Fig. 3 may be approximated by three different analytical expressions for the correlation area, corresponding to "low," "intermediate" and "large" values of $k_p(U_c/U_1)\delta_1$. The intermediate range corresponds to the condition already considered, i.e.,

$$A_t \propto \delta_1^2 \propto z_{1/2}^2 \qquad (2.18)$$

where δ_1 is the equivalent boundary-layer displacement thickness. The shaping of the power spectrum at low and high frequencies will be controlled by the expressions for A_t at low and high values of $k_p(U_c/U_1)\delta_1$, respectively. U_c is the turbulence convection velocity, and the ratio U_c/U_1 is assumed constant.

a) At low values of $k_p(U_c/U_1)\delta_1$,

$$A_t \propto k_p^2 \delta_1^4 , \qquad (2.19)$$

where k_p, the wavenumber for flexural waves in the panel, is proportional to $\sqrt{\omega/h}$.

Placing this expression for A_t into Eq. (2.16), applying suitable limits and solving the integral, we obtain an expression of the form

$$\Pi \propto \frac{U_m^5 z_{1/2}^3 R_1^2}{h^3} \ln (1 + k_d^4 r_2^4) \qquad (2.20)$$

where $k_d^2 = 5\omega z_{1/2}/R_1^2 U_m$. Equation (2.20) indicates a weak dependence of power on frequency. It is interesting to note the change in the dependence of the power upon the flow parameters U_m and $z_{1/2}$ and, particularly, the cubic dependence upon the plate thickness, as opposed to the square dependence which occurs in the middle frequency range.

b) At large values of $k_p(U_c/U_1)\delta_1$,

$$A_t \propto k_p^{-4} \delta_1^2 . \qquad (2.21)$$

Using this dependence in Eq. (2.16), we find

$$\Pi \propto U_m^2 R_1^2 \left[\frac{1}{k_d^2 r_1^2} - \text{Arctan}\left(\frac{1}{k_d^2 r_1^2}\right)\right] . \qquad (2.22)$$

The frequency-dependence of the power in this expression is quite strong, ranging from about 3 dB per octave at the lower frequencies to about 9 dB per octave in the upper experimental range. It is interesting to note that the power supplied to the test panel is no longer dependent upon the panel thickness. Thus we might expect the power curves for different thicknesses of panel to converge at the higher frequencies. This behavior is observed in the experimental studies.

2.6 Experimental Studies

2.6.1 Wall-Jet Equipment

The basic airflow equipment used in these experiments forms part of the high-intensity siren facility at BBN. This equipment is capable of supplying 6000 standard cfm of air at pressures up to 14 psi. The major modifications to the siren facility have consisted of removing the sirens and ducting the outlet air from the aftercooler along the axis of the concrete horn into the termination room. A portion of this duct has been acoustically treated to minimize the acoustic (as opposed to the aerodynamic) excitation of the test panel by upstream noise sources. The muffler takes the form of a three-inch-thick lining of Fiberglas, faced with hardware cloth, within a twelve-foot-long and twelve-inch-diameter portion of the air duct. The attenuation provided by this muffler is in excess of 25 dB over the frequency range of interest. The last eight feet of the ducting system consists of a 1-5/8-inch-diameter steel tube fitted with a six-inch-diameter steel flange to help form the jet. The jet dimensions are similar to those employed by Hodgson.

The jet impinges normally onto a six-by-four-ft flat aluminum panel. The panel is held in a vertical plane parallel to the plane of the jet flange. It is secured at four points to wooden battens fixed between the floor and the ceiling of the termination room. Throughout the experiments, the spacing between the flange and the plate was fixed at 5/8 inch. At different stages in the studies 1/16-inch and 3/16-inch-thick panels were used. Two thicknesses were chosen so that the effect of a change in input panel impedance on the amount of power which the panel would accept from the turbulent wall-jet might be observed. Both test panels were lightly treated with damping tape to improve the diffuseness of the reverberant vibrational field.

2.6.2 Average Velocity Profile Measurements

The preceding analysis has shown that the aerodynamically generated excitation forces acting on the panel depend upon the mean flow velocity maximum, U_m, and upon the distance to the half-velocity point, $z_{1/2}$, at some arbitrary distance, R_1, from the axis of the wall-jet.

These flow parameters were measured using a pitot tube at a radius of 4.25 inches. In spite of a tendency for the panel to flex as the mean flow velocity of the wall-jet increased, no significant change in the distance to either the velocity maximum, z_m, or to the half-velocity point, $z_{1/2}$, was observed as the flow velocity was changed. The value of z_m could only be approximated on account of the thinness of the inner layer and the roundness of the velocity profile in the region of peak velocity. The profile measurements made in the present study are tabulated below together with comparable data by Hodgson. In general, the agreement is reasonably good.

TABLE IV

AVERAGE VELOCITY PROFILE MEASUREMENTS

	Flange Diameter	Flange/Plate Spacing	R_1	z_m	$z_{1/2}$
BBN	6 in.	0.625 in.	4.25 in.	0.1 in.	0.35 in.
Hodgson	6 in.	0.75 in.	4.25 in.	0.07 in.	0.32 in.

Three settings of flow velocity were used, corresponding to values of U_m at the chosen radius of 56, 155 and 290 ft/sec.

The flow profile information, together with knowledge of the material properties and thickness of the test panel, provides us with sufficient data to compute the theoretical power accepted by the panel from the wall-jet.

2.6.3 Measured Power into Test Panel

In this experimental study the actual power accepted by the test panel is measured and compared with the power predicted by the theoretical analysis.

The rate of energy flow into the panel is given by the relation

$$\Pi_m = \omega \eta M \overline{v^2} \qquad (2.23)$$

where M is the mass of the panel, $\overline{v^2}$ the measured mean square velocity and η the loss factor.

The panel response was measured using a Gulton Glennite Type 314 Accelerometer. The useful range of the accelerometer extends to 12 kHz. Measurements were taken at a number of positions to obtain a spatial average for the mean-square velocity. The loss factor was derived from measurements of the reverberation time, T_R, using the relation

$$\eta = 2.2/T_R f \qquad (2.24)$$

where f is the frequency of excitation. All these measurements were made in third-octave filter bands over the frequency range of 250 Hz to 10,000 Hz.

2.7 Experimental Results

Experimental results are summarized in Figs. 12 and 13 for peak profile velocities of 155 and 290 ft/sec, respectively. Each figure describes the measured power, Π_m, in the two panels of different thickness as a function of frequency. The experimental data in these figures give only partial support to the theoretical calculations. The data in the lower frequency ranges do tend to show an approximate 10-dB separation between the curves, as would be expected from the difference in input conductance of the two plates used. Also, after the roll-off at higher frequencies, the power tends to be independent of plate thickness, as anticipated by the theory.

In Fig. 14, we show additional input power data, with the flow parameters described by volume flow and pipe diameter. In this data, the flange-to-plate spacing has been increased so that the effect of the flange on the wall-jet has been minimized. The better agreement between theory and data in this figure than that obtained in Figs. 12 and 13 suggests that the flange is detrimental to wall-jet development.

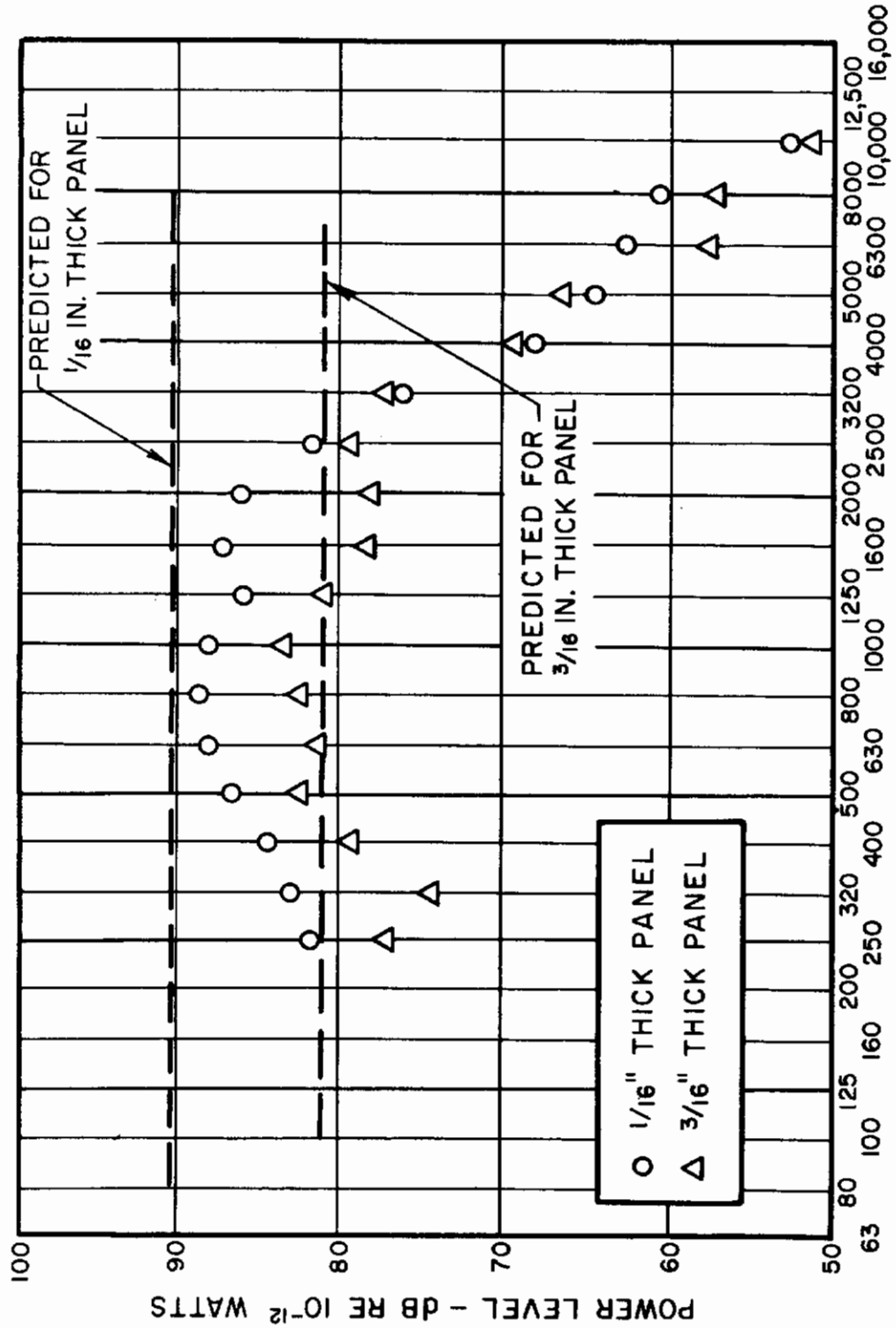

FIG. 12 EXCITATION OF PANEL BY WALL-JET, U_m = 155 ft/sec, SHOWING MEASURED POWER LEVELS AND PREDICTED LEVELS AS MEASURED BY SIMPLE THEORY

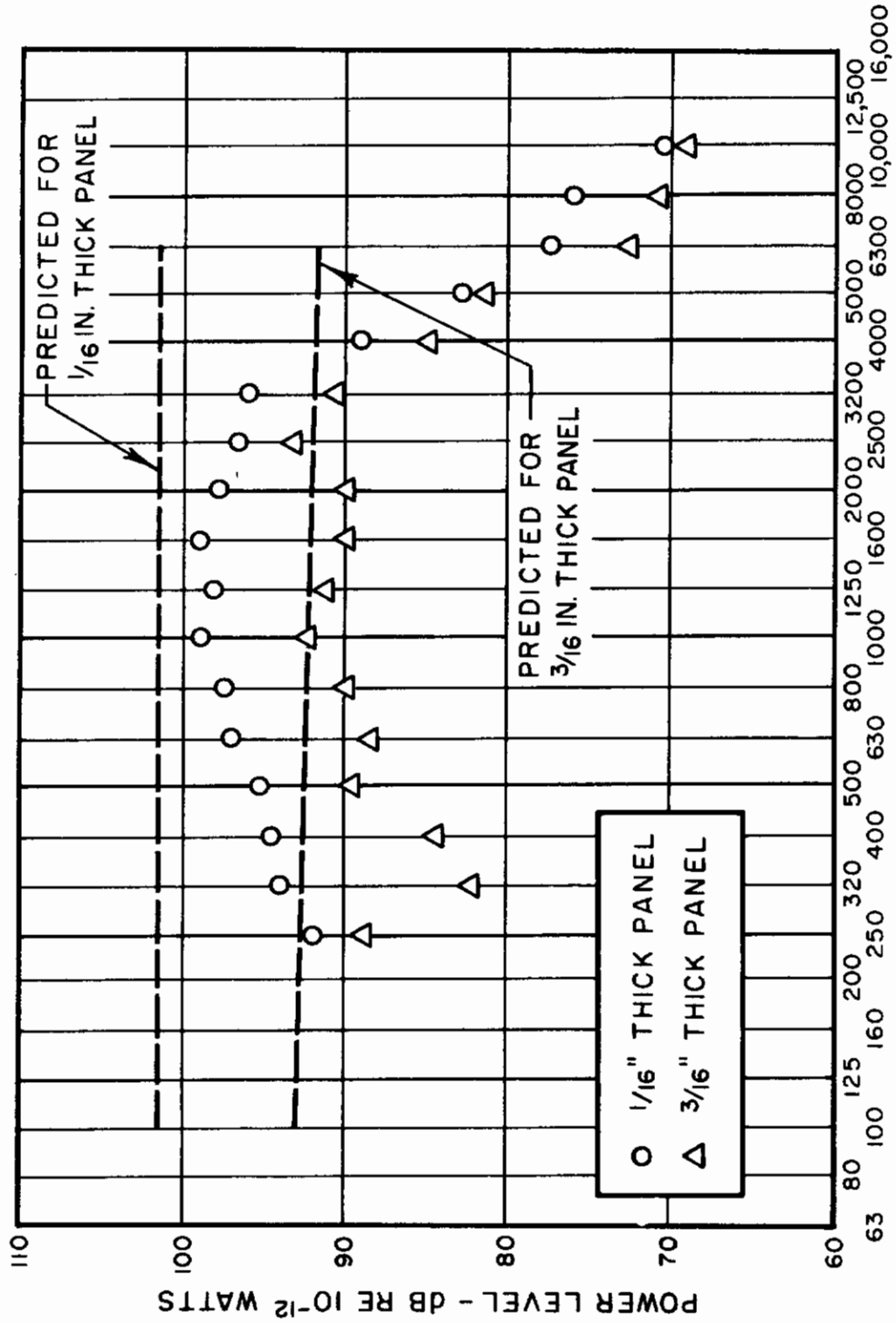

FIG. 13 EXCITATION OF PANEL BY WALL-JET, U_m = 290 ft/sec, SHOWING MEASURED POWER LEVELS AND PREDICTED LEVELS AS MEASURED BY SIMPLE THEORY

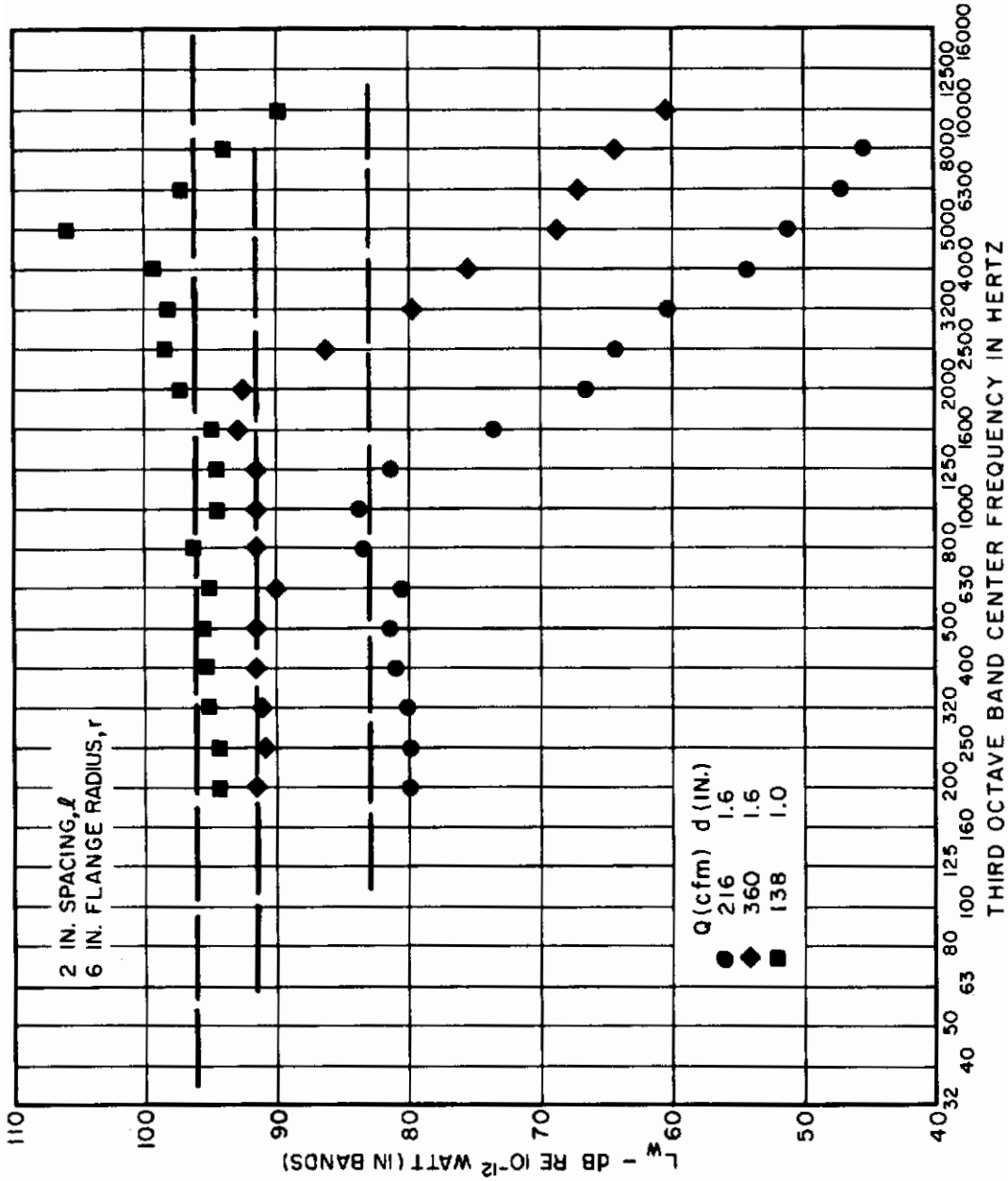

FIG. 14 POWER ABSORBED BY 1/16 IN. ALUMINUM PLATE EXPOSED TO WALL-JET. DASHED LINES ARE THEORETICAL CALCULATIONS, DATA POINTS ARE FOUND FROM REVERBERANT ACCELERATION LEVEL ON PLATE AND LOSS FACTOR

PART II. SIMULATION OF TURBULENT BOUNDARY LAYER WITH WALL-JETS.

3. INTRODUCTORY COMMENTS

In Part I of this report we have described the turbulent boundary layer as a source of mechanical excitation of an aircraft structure. The calculations were applied to estimation of the mechanical power absorbed by panels in the rearward sections of a large supersonic aircraft flying a mission profile characteristic of that planned for the supersonic transport (SST) (Ref.9).

An unexpected feature of the power spectra was their similarity in shape and level for different periods of the flight profile. This suggests that an experiment showing the feasibility of replacing the actual turbulent boundary layer environment with a collection of wall-jets for an average set of flight parameters should establish a fair degree of confidence that the environment can be simulated for the entire mission. It is the purpose of Part II of this report to develop such a simulation scheme for a major structural section of an aircraft. This scheme will, in effect, result in the design of an experiment to evaluate the effectiveness of a set of wall-jets used to simulate TBL response.

4. DESCRIPTION OF THE EXPERIMENTAL MODEL

4.1 Selection of Structural Parameters

The structural section selected for the simulation should satisfy these major criteria:

(a) It should be sufficiently large so that the effects of its detachment from the rest of the structure are minimal and so that noise and vibration response measurements can be conveniently made.

(b) It should consist of panel-frame elements using dimensions, geometry, and materials appropriate to a structure of current interest.

(c) It should be representative of a section of the aircraft where TBL excitation is high and might be expected to be bothersome.

On the basis of these criteria, we have chosen to study the structural configuration shown in Fig. 15. It is a cylinder 10 ft in diameter and 30 ft long. It is formed of stringers and ring frames, 1.5 ft on centers, supporting 50-mil titanium panels, and represents a possible configuration of an aft portion of the SST. We next estimate typical levels of power absorbed by this structure during a representative portion of the flight profile, and subsequently consider the problem of achieving an excitation of the structure that is as spatially uniform as that provided by the TBL.

4.2 Selection of the Power Levels to be Achieved

In section 1, we described a method of predicting the power absorbed by a panel from convected turbulence. The results were expressed as power input in one-third-octave bands per unit area of the panel. The power absorbed from the TBL was computed for various segments of an assumed flight profile of the SST for a 50-mil flat titanium panel.

Fig. 16 shows a representative curve illustrating the band power levels to be achieved in order to simulate a Mach 2 portion of the flight. This curve is obtained by drawing a smooth curve through the Mach 2 estimate for a 1-sq ft panel in Fig. 7 and increasing it by 30 dB to convert to a 1000-sq ft structure. Referring to Fig. 7, we see that this curve is representative of the higher excitation levels and should provide a good test of our ability to simulate the TBL environment.

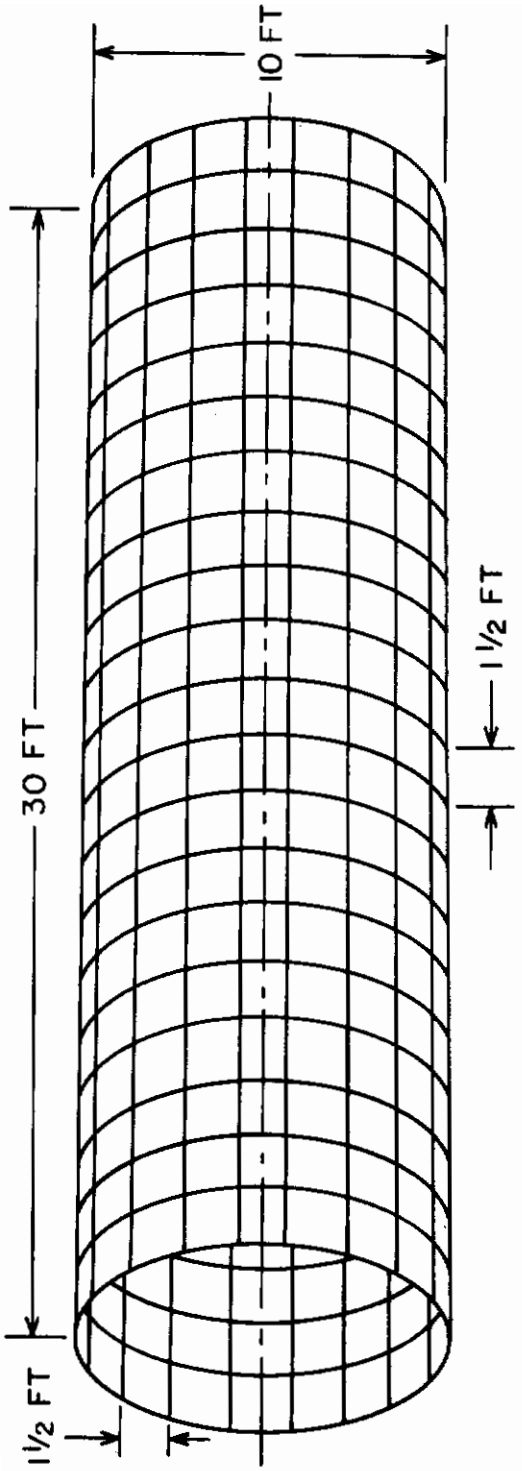

FIG. 15 DIAGRAM OF TEST STRUCTURE USED IN TBL SIMULATION STUDY

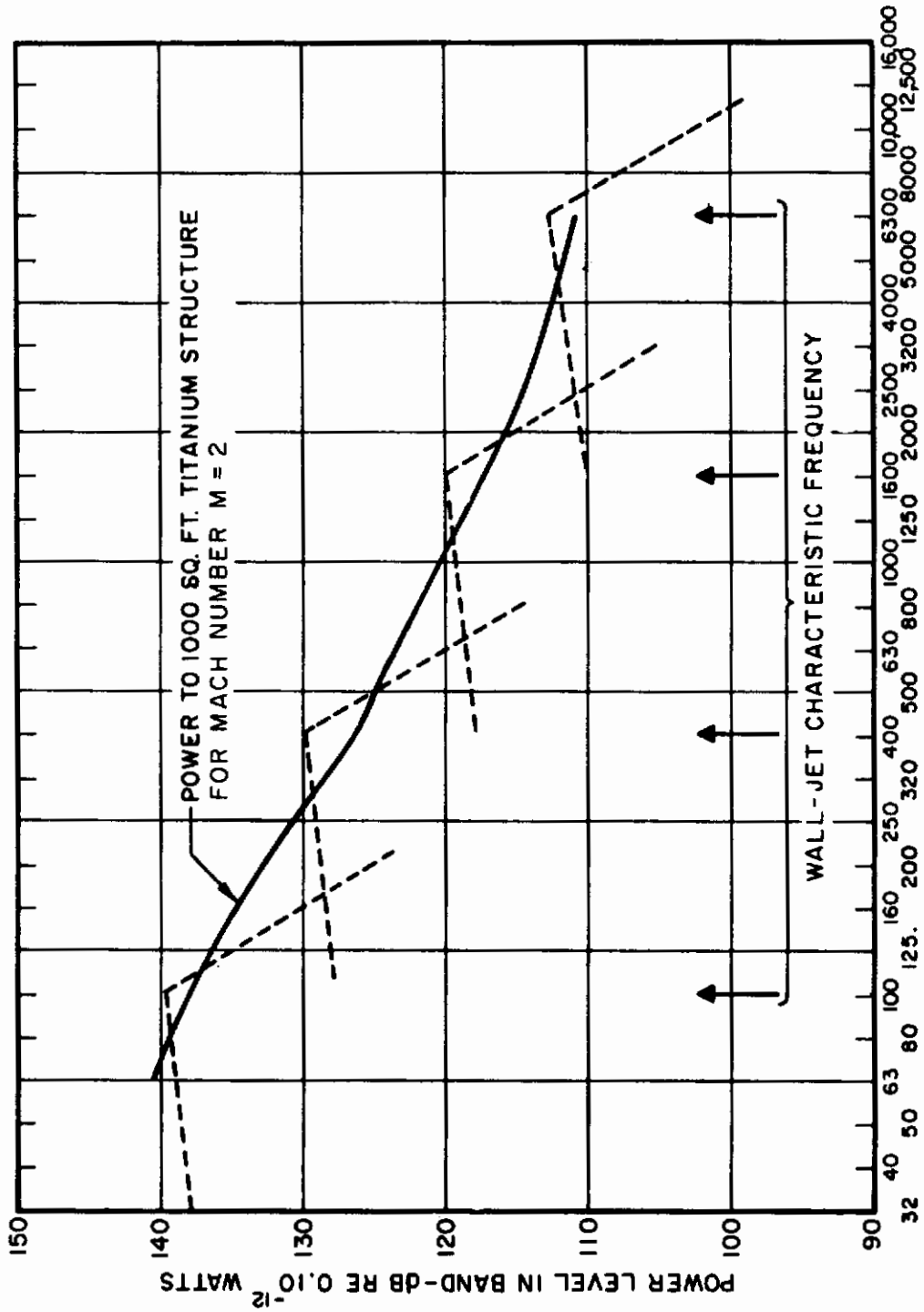

FIG. 16 SIMULATION OF BOUNDARY LAYER NOISE EXCITATION USING FOUR WALL-JETS OF FOUR SIZES

4.3 Effect of Frames and Stringers on Homogeneity of Response

Some devices, such as wall-jets, which will inject controlled amounts of mechanical power into a structure, do so over a fairly small region of the structure. If the spatially homogeneous excitation of a TBL is to be simulated, it must be possible for the mechanical energy to spread over the structure without too much hindrance. This means that either we supply energy directly to each panel (which requires very many jets) or we rely on transmission across panel boundaries. The purpose of this section is to present two calculations of vibrational level inhomogeneity for different densities of jets over the surface.

In Fig. 17, we show the pattern of excitation when every other panel is directly excited with a wall jet. The dashed lines indicate boundaries of symmetry across which there is no average energy flow. The energy ratio can therefore be obtained by considering only a pair of triangular sections of the structure, labeled (1) and (2) in Fig. 17. For a two-element structure like that shown, the modal energy ratio is (Ref. 23)

$$\frac{E_2}{E_1} = \frac{\eta_{21}}{\eta_{21} + \eta_2}, \qquad (4.1)$$

where E_2 and E_1 are the modal energies of the receiving and excited plates, respectively, η_2 is the internal loss factor of plate 2, and η_{21} is the loss factor of plate 2 due to transmission into plate 1. The definitions and interpretations of these parameters are developed in Reference 23.

The loss factor η_2 can be determined by measurement on the real structure, but we shall assume that it has the constant value of 0.01. The coupling loss factor for transmission of energy past a supported line on a panel will be used for η_{21}. This is computed from the general relation (Ref. 24)

$$\eta_{coup} = 4/3\pi\, k_p\, D, \qquad (4.2)$$

where $k_p = 2\pi/\lambda_p$ is the flexural wavenumber in the panel (λ_p is the flexural wavelength), and $D = \pi A/P$ is the mean free

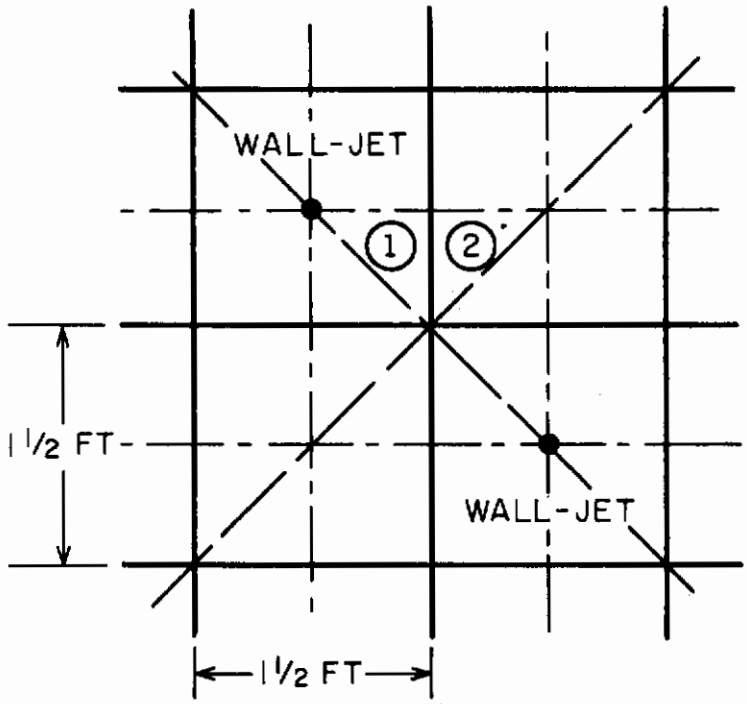

FIG. 17 WALL-JET LOCATIONS WHEN EVERY OTHER PANEL IS DIRECTLY EXCITED

path of the panel where A is its area and P is the length of the energy-transferring boundary.

For the panel in Fig. 17, $d = \frac{3}{8}\pi$ ft. Using the simplified relation

$$\lambda_p = 50\sqrt{h/f} \quad \text{ft} \tag{4.3}$$

where the plate thickness h is in inches and f is in Hz, the coupling loss factor η_{21} is readily computed. Using the assumed value of η_2, we have computed 10 log (E_2/E_1) and the results are shown in Fig. 18. The results indicated that a 3-dB variation from excited to non-excited panels may occur at the very high frequencies.

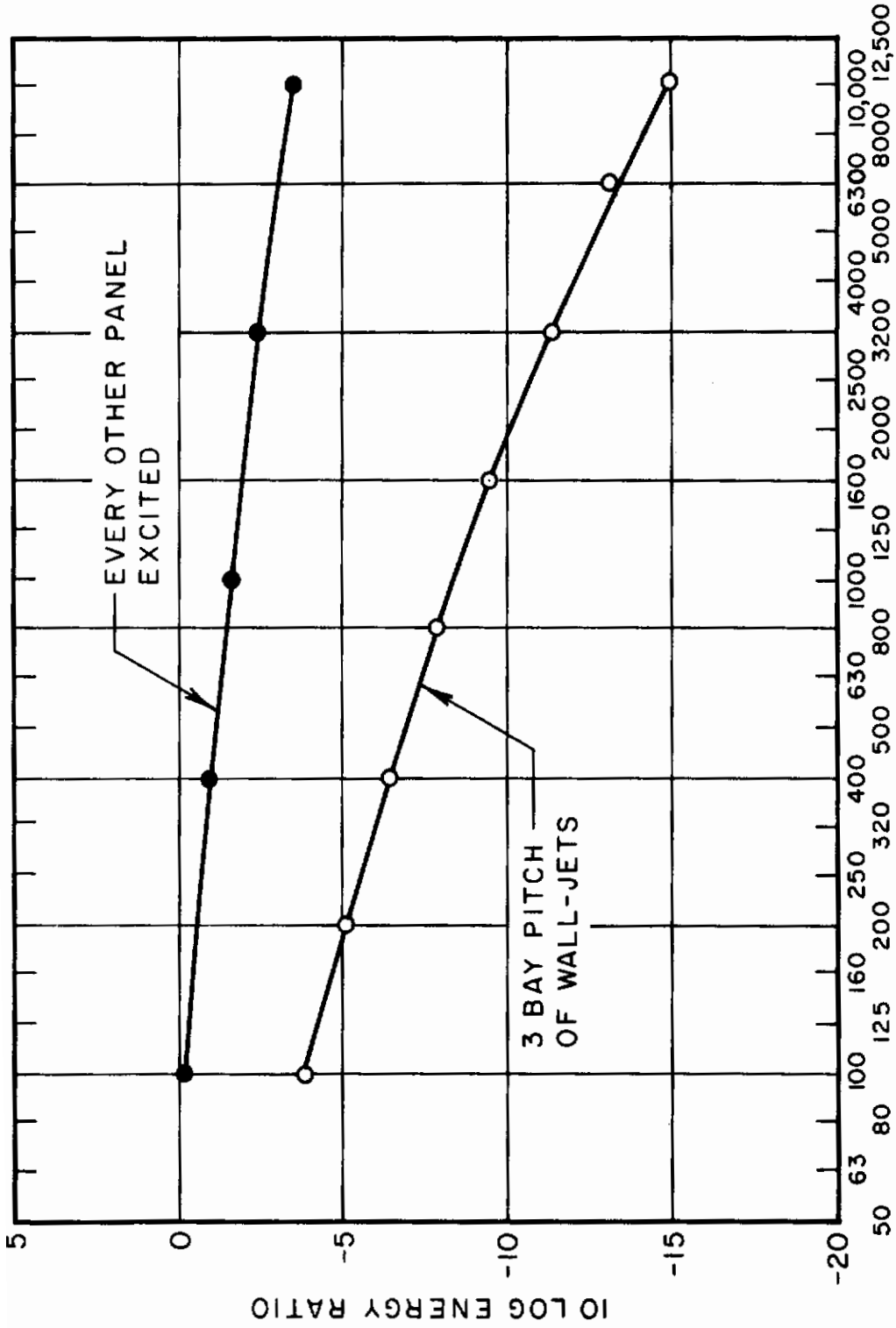

FIG. 18 ENERGY INHOMOGENEITY WITH WALL-JET EXCITATION

Fewer wall jets will be necessary if they are spaced at a pitch of 3 bays, as shown in Fig. 19. The diagram again shows dashed lines across which energy is not expected to flow, and heavy lines indicate energy-transfer boundaries. The ratio of energy in the corner panel section, E_3, to that of the wall-jet excited section, E_1, may be written as (Refs. 25 and 26)

$$\frac{E_3}{E_1} = \frac{n_3}{n_1} \frac{\eta_2^3}{\eta_2 + \eta_3^2} \frac{\eta_1^2}{\eta_2 + \eta_2^1 + \dfrac{\eta_2^3 \eta_3}{\eta_3 + \eta_3^2}}, \qquad (4.4)$$

where $\eta_{i\pm1}$ is the loss factor for dissipation in the i^{th} panel and $\eta_i^{i\pm1}$ is the coupling loss factor for the power flowing from the i^{th} panel to the $(i\pm1)^{th}$ panel. In addition, there is a relation between η_i^{i+1} and η_{i+1}^{i} given by (Ref. 24)

$$n_{i+1}\, \eta_{i+1}^{i} = n_i\, \eta_i^{i+1} \qquad (4.5)$$

where n_i is the modal density of the i^{th} panel. We assume $\eta_i = 10^{-2}$ as a typical value of loss factor for all panels. The modal density is given by (Ref. 27)

$$n_i(f) = \frac{A_i}{h_i} \times 10^{-4} \qquad (4.6)$$

where A_1 is in sq ft and h_1 is in ft. The coupling loss factors are given by Eq. (4.2). The areas of the panels in our section vary so that $4n_1 = n_2 = n_3$. Choosing a frequency of 2000 Hz as typical for the region of interest, and for a panel 1/16 inch thick, Eq.(4.6) gives $\eta_2^3 = 8 \times 10^{-3}$. From Eq. (4.5) we find $\eta_2^3 = \eta_3^2 = \frac{1}{2}\eta_1^2 = 2\eta_2^1$. The energy ratio from Eq. (4.4) is 0.1, which corresponds to a level in the corner panel about 10 dB lower than in the panel excited directly by the wall jet. The ratio (4.4) is shown as a function of frequency for a constant $\eta_1 = 10^{-2}$ in Fig. 18. At higher frequencies we would probably conclude that the inhomogeneity of response is too great to allow confidence in the results derived from the simulation of Fig. 19.

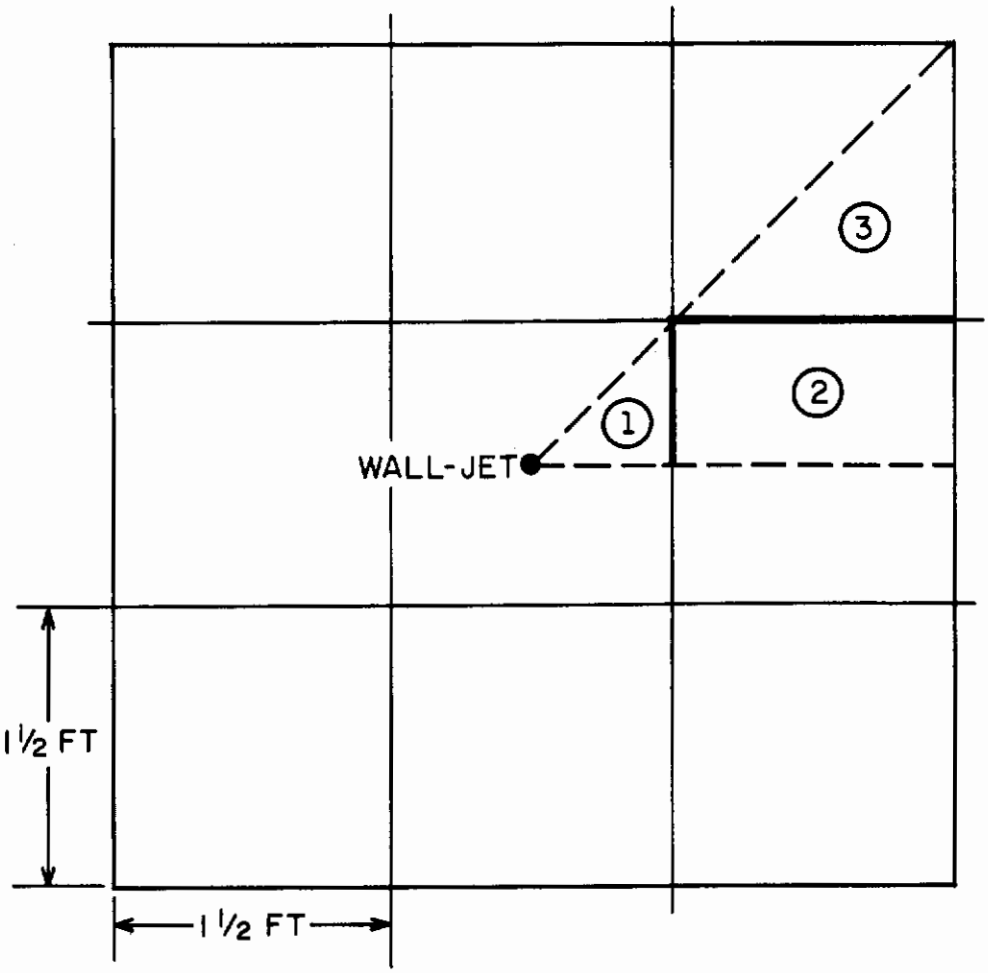

FIG. 19 TYPICAL SECTION OF THE STRUCTURE SHOWING THE AREA EXCITED BY ONE WALL-JET

5. THE APPLICATION OF WALL JETS AS SOURCES OF BROADBAND MECHANICAL EXCITATION

In section 2, we computed the frequency spectrum of input power to a structure anticipated as a result of boundary-layer excitation. In addition, we showed that appropriate levels of excitation can be produced by employing a number of wall-jets distributed over the surface of the structure.

In order to apply wall-jets to TBL simulation, we must be able to control the basic spatial and temporal parameters. In particular, we must derive an empirical relation between the geometry and flow in the wall-jet and the frequency at which the input power to the plate reaches a maximum level. In addition, we must relate wall-jet flow parameters (U_m and $z_{1/2}$) with more easily measured quantities in the jet pipe. Such relations allow us to design a spectrum shape and level on the basis of pipe flow parameters (volume flow and diameter) alone.

5.1 Experimental Studies of Parameter Dependence

In the earlier experiments, the geometry of the wall-jet was maintained constant while the plate thickness and flow velocity were varied. However, in subsequent experiments the nozzle- or flange-to-plate spacing, the flange diameter, the jet pipe diameter, and the flow speed have been varied while the plate thickness was kept constant. It is our intent in this section to summarize the principal findings of our work so that we can formulate a tentative set of parameter relationships. A working system for the simulation of boundary layer noise excitation of a structure using wall jets can then be designed.

In Section 2, the calculations of input power to a plate excited by a wall jet have generally given a good estimate of the maximum levels of panel excitation to be expected, but they have not clarified the source of a rather abrupt high-frequency cutoff. An attempted explanation, on the basis of assuming a finite minimum radius of the wall jet, gave the wrong cutoff frequency and rate of drop-off in spectrum.

The effect of the flange in defining the wall-jet shape has been clarified by an experiment in which $z_{1/2}$ was measured at a fixed radius R and the flange-to-wall spacing ℓ was varied. The results, shown in Fig. 20 indicate that, for small spacings, ℓ does control the jet thickness, but when ℓ exceeds 20% of the pipe diameter d, the jet thickness $z_{1/2}$ does not vary significantly. A sizable amount of the data reported in section 2 was taken, therefore, on a wall-jet for which the flange had only a minimal effect on the jet parameters.

5.2 Peak Power Levels

On the basis of the theoretical expressions for power developed in section 2, and using a "best-fit" value of correlation area A_t, the power flow to a plate per unit area from the impinging wall-jet is given by

$$\Pi = 10 \log \left[1.14 \times 10^{5} \, U_m^4 \, z_{1/2}^2 \, R^2/h^2 \sqrt{E\rho_p} \right] \quad (\text{dB re } 10^{-12} \text{ watts}) \qquad (5.1)$$

where U_m(ft/sec) and $z_{1/2}$(ft) describe the peak and width of the wall-jet velocity profile at an arbitrary radius R(ft); h(ft) is the thickness of the plate; and E(psf) and ρ_p(lb/ft^3) are the Young's modulus and density of the plate material, respectively. It appears that, on the basis of experimental data, this expression will give a good estimate of the maximum levels of panel excitation over a fairly wide range of jet parameters.

5.3 Frequency Spectrum

Our experimental studies have shown that, when the jet/plate spacing is of the order of a jet-pipe diameter or greater, the shape of the spectrum is constant, having a slope of about 2 dB per octave below a characteristic frequency and about -15 dB/ octave above this cutoff frequency.

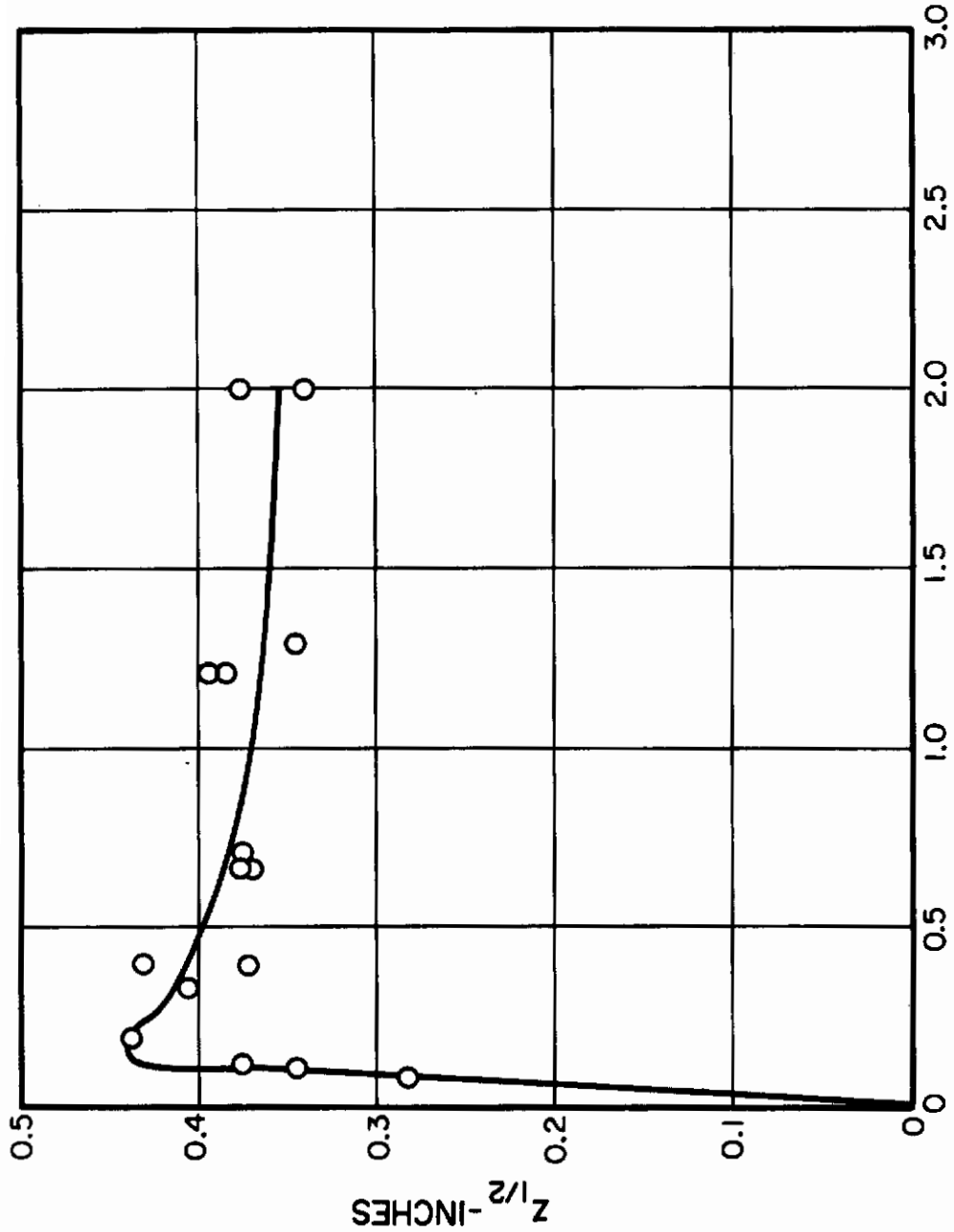

FIG. 20 EFFECT OF FLANGE-TO-PLATE SPACING ON WALL-JET THICKNESS

In Fig. 21, we show the measured values of the cutoff frequency in several experiments. They are plotted against a characteristic pipe flow frequency V/d, where V is the average flow speed in the pipe and d is the pipe diameter. We note that there is a fairly direct relationship when the flange-to-plate separation satisfies the condition $\ell/d>0.8$:

$$f_{co} = 0.6\ V/d \quad . \tag{5.2}$$

Other factors seem to dominate at smaller separations. This is consistent with the results of Fig. 20, which indicated that the flange "loses control" over the wall jet when $\ell/d>0.8$ and that other parameters, such as pipe diameter, become dominant in defining $z_{1/2}$.

5.4 Wall-Jet Parameters and Volume Flow

As we have seen, the width of the wall-jet velocity profile $z_{1/2}$ becomes independent of the jet/plate spacing when the spacing equals or exceeds about one jet-pipe diameter. Although no experimental verification has been obtained, it would seem probable that, under these conditions, $z_{1/2}$ will depend upon the diameter of the jet-pipe as well as upon the radial distance from the jet axis. An empirical relation consistent with available data is

$$z_{1/2} = 0.625\ Rd \tag{5.3}$$

where $z_{1/2}$, R and d are all in ft.

On an experimental basis, quantities such as U_m and $z_{1/2}$ are inconvenient since they require measurements of the flow profile. We would much prefer to relate the power level and cutoff frequency to parameters like pipe diameter d, pipe-to-wall spacing ℓ, and average pipe flow speed V (or volume flow $Q = V\pi d^2/4$).

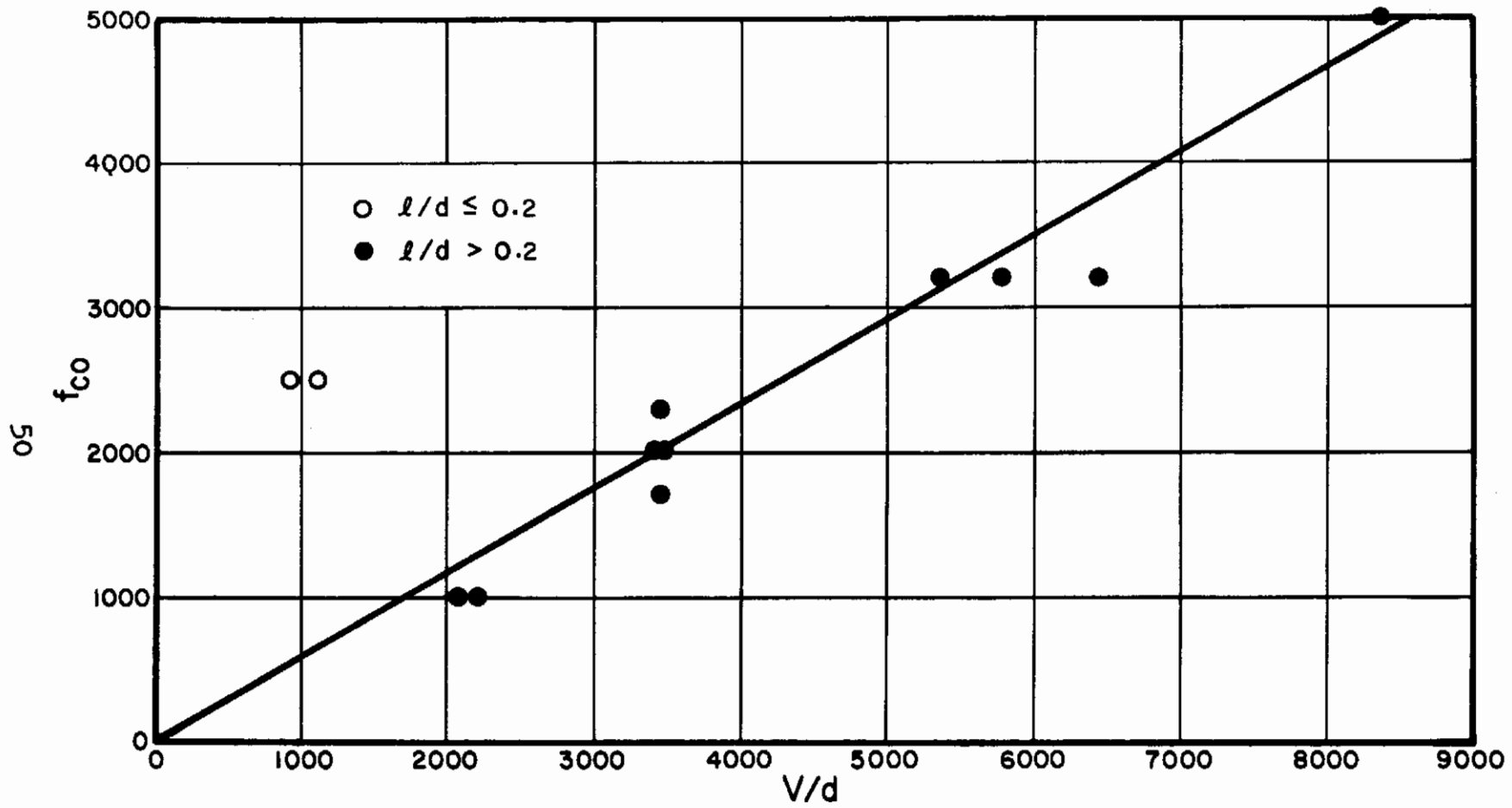

FIG. 21 CUTOFF FREQUENCY AS FUNCTION OF JET GEOMETRY

Consider a wall-jet operating in a regime where the flange has no effect on the flow configuration, as was shown in Fig. 8. If little mixing occurs, the volume flow in the jet may be assumed to be preserved until a position A, where mixing becomes appreciable and the wall-jet "begins." From dimensional considerations, we expect the diameter of this transition line to be proportional to d, and the volume flow per unit length along this line to be proportional to $U_m z_{1/2}$, which is preserved in the mixing region of the jet. Accordingly, we expect Q to be given by

$$Q = \text{const. } d\ U_m\ z_{1/2}. \qquad (5.4)$$

In Fig. 22 we show a plot of volume flow versus $d\ U_m\ z_{1/2}$ based on several experiments using different pipe diameters, flow speeds, and pipe-wall separations. The best data fit occurs when the constant in Eq. (5.4) is taken to be 7.5.

The empirical Eqs. (5.1) to (5.4) describe the power, the frequency and the flow parameters of the wall-jet excitation in a sufficient manner to enable us to develop tentative working formulas for a full-scale boundary-layer simulation experiment. We must stress the tentative nature of these formulas, however, since the range of parameters used in our studies has in many instances been too small to allow their complete verification.

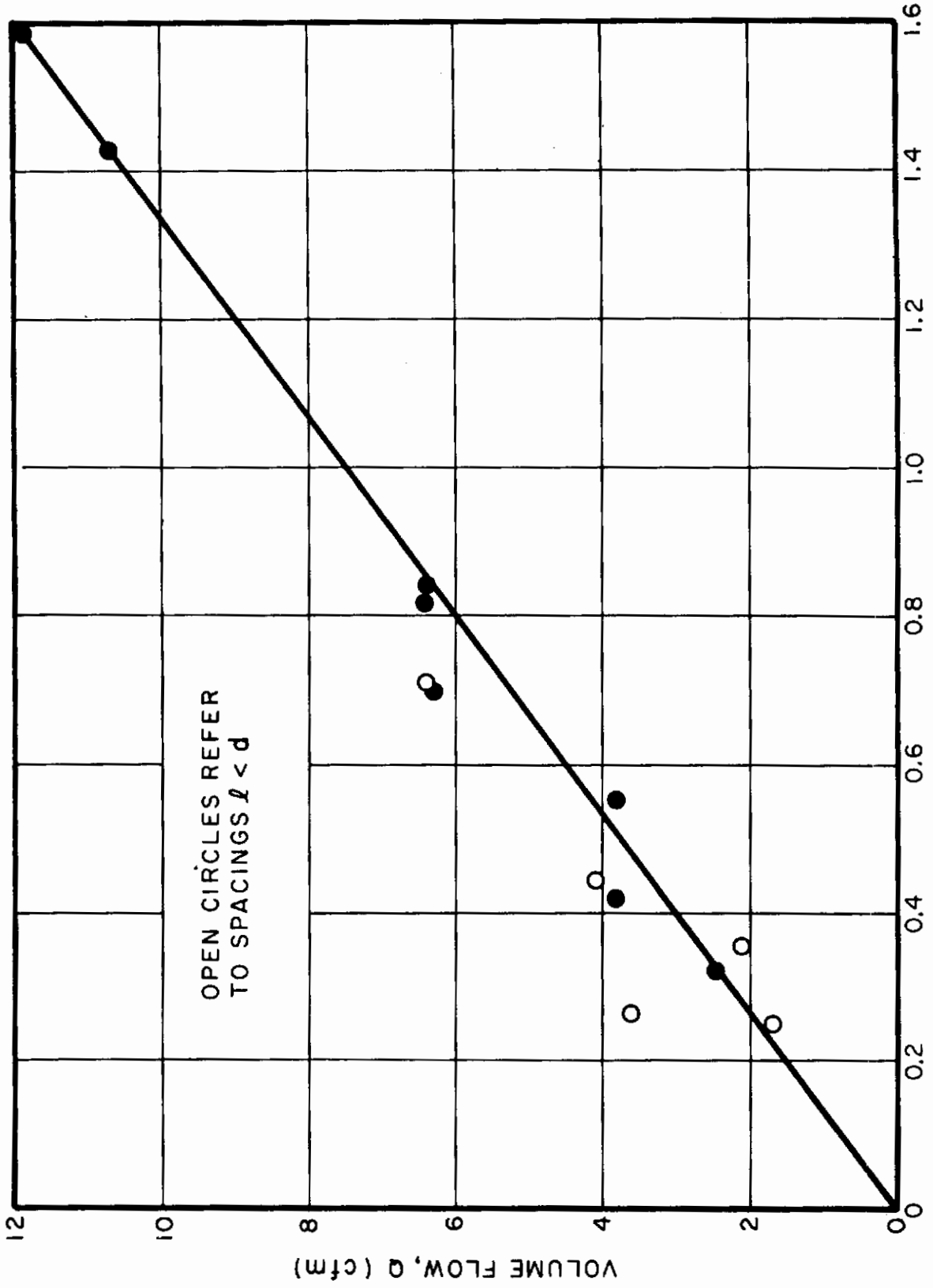

FIG. 22 VARIATION OF VOLUME FLOW WITH WALL-JET PARAMETERS

6. DESIGN OF A SIMULATION EXPERIMENT

As an example of the design of a full-scale simulated boundary-layer excitation experiment, we shall use the hypothetical structure considered in section 4. This structure is a 30-ft-long section of an aircraft fuselage having a total surface area of about 1000 sq ft. We also assume a representative panel structure of titanium alloy, 0.05 in. thick. This latter assumption allows us to make use of the computations of anticipated power contained in section 4.

The anticipated input power to this structure from boundary-layer excitation (for a Mach number M = 2) is shown in Fig. 16. This is the power spectrum which we wish to simulate using a distribution of wall-jets. Superimposed on this spectrum we show the characteristic power spectra for four different sizes of wall-jet, arranged to provide the necessary simulation. The wall-jet requirements are therefore as follows:

TABLE V

WALL-JET REQUIREMENTS

Jet System No.	Peak Power Level dB re 10^{-12} watts	Characteristic Frequency H_z
1	113	6300
2	120	1600
3	130	400
4	140	100

By manipulation of Eqs. (5.1) to (5.4), and by insertion of the appropriate values relating to titanium panels 0.05 in. thick, the following equations are derived:

$$\Pi = 10 \log (1.65\ NV^6/f_{co}^2) \qquad (6.1)$$

$$d = 0.6V/f$$

where N is the number of wall-jets of identical size used to simulate the part of the power spectrum of cutoff frequency f_{co}. The values of Π and f_{co} are derived from the power spectrum which we wish to simulate. The minimum value of N follows from considerations of the transfer of energy throughout a multi-panelled structure developed in section 4. Thereafter the values of V and d are uniquely described.

In Table VI we show the appropriate pipe velocities and diameters, and total volume flow associated with each jet system required to reproduce the power spectrum shown in Fig. 16, and described in Table V. The requirements are based on 200 and 40 jets per system (the two jet layouts represented in Figs. 17 and 19, respectively).

Both in terms of jet-pipe diameters and air-flow requirements, the simulation of the boundary-layer excitation spectrum for frequencies below 1000 Hz would appear to be impractical, since the maximum air flow capability of the Sonic Fatigue Facility at Wright-Patterson Air Force Base is 300,000 cfm.

TABLE VI

DESIGN REQUIREMENTS FOR PIPE VELOCITIES, DIAMETERS AND TOTAL FLOW

	N = No. of jets/system					
	N = 40			N = 200		
f_{co}	V (ft/sec)	d (inches)	total Q cfm	V ft/sec	d inches	total Q cfm
6300	610	0.725	4,200	465	0.55	9,300
1600	570	2.67	53,000	435	2.04	117,200
400	530	9.9	682,000	405	7.55	---
100	490	36.8	---	374	28.0	---

7. CONCLUSIONS AND RECOMMENDATIONS

The theoretical and experimental analyses presented in this report indicate that the air-flow capability of the Sonic Fatigue Facility can be applied to the simulation of TBL-induced vibration and noise at higher frequencies. The simultaneous use of wall-jets for high-frequency simulation and a sound field for lower-frequency excitation combines the advantages of both systems.

The wall-jet has many interesting features as a source of broadband mechanical excitation. The present study has only begun to explore its capabilities and operational parameters. As a result of this study, however, we believe that the wall-jet can become a valuable tool in the arsenal of controlled environmental sources for the acoustical and structural engineer.

REFERENCES

1. Hilton, D. A., W. H. Mayes, and H. H. Hubbard, "Noise Considerations for Manned Re-Entry Vehicles," NASA TN D-450, September 1960.

2. Wilmarth, W. W., and C. E. Wooldridge, "Measurement of the Fluctuating Pressure at the Wall Beneath a Thick Turbulent Boundary Layer," University of Michigan, Office of Research Administration Report, April 1962.

3. Maidanik, G., and E. M. Kerwin, Jr., "Acoustic Radiation from Ribbed Plates Including Fluid Loading Effects," BBN Report No. 1024, submitted October 1963 to Bureau of Ships.

4. Dyer, I., "Sound Radiation into a Closed Space from Boundary Layer Turbulence," BBN Report No. 602, submitted 12 December 1958 to Office of Naval Research, USN. Also, reference 5.

5. Ffowcs Williams, J. E., and R. H. Lyon, "The Sound Radiated from Turbulent Flows near Flexible Boundaries," BBN Report No. 1054, submitted 15 August 1963 to Office of Naval Research, USN.

6. Ibid., p. 11.

7. Ibid., Figure 4.

8. Lyon, R. H., "Panel Excitation by High Speed Boundary Layer Turbulence," 67th Meeting of the Acoustical Society of America, 6-9 May 1964, New York, Paper W3. The response of an infinite panel to convected, non-decaying turbulence has been previously computed by H. S. Ribner, "Boundary Layer Induced Noise in the Interior of Aircraft," UTIA Report No. 37, April 1956.

9. Goodmanson, L. T., W. T. Hamilton and M. L. Pennell, Paper No. 4, (U) Proceedings of NASA Conference on Supersonic-Transport Feasibility Studies and Supporting Research, September 1963 (CONFIDENTIAL Report).

10. U. S. Standard Atmosphere, 1962, NASA, USAF, USWB, December 1962.

11. Kistler, A. L., and W. S. Chen, "The Fluctuating Pressure Field in a Supersonic Turbulent Boundary Layer," Jet Propulsion Laboratory, Report No. 32-277, August 1962.

12. Ibid., Figure 1.

13. Hilton, D. A., E. M. Bracalente and H. H. Hubbard, "In-Flight Aerodynamic Measurements on a Scout Launch Vehicle," NASA Technical Note D-1818, July 1963.

14. Schlichting, H., Boundary Layer Theory, McGraw-Hill Book Company, New York, 1955 (translated by J. Krestin).

REFERENCES (continued)

15. BBN Memorandum to Douglas Aircraft Company, Inc., "A Brief Investigation of Flight and Wind Tunnel Measurements of Boundary Layer Pressure Fluctuations," 9 November 1964.

16. Ibid., Figure 6.

17. Lyon, R. H., "Boundary Layer Noise Response Simulation With a Sound Field," Paper presented at the Second International Conference on Acoustical Fatigue, 1964.

18. Ibid., Strictly speaking, Fig. 3 is only an approximation to the A_t for the HC regime that is more precisely specified in reference 17.

19. Glauert, M. B., "The Wall Jet," J. Fluid Mech., 1, 6, 625 (1956).

20. Hodgson, T. H., "Pressure Fluctuations in Shear Flow Turbulence," College of Aeronautics Note 129, Cranfield, England.

21. "Boundary Layer Noise Induced Vibration and Its Simulation in the ASD Sonic Fatigue Facility," BBN Proposal P64-E-1, submitted 26 July 1963 to ASD. Appendix I.

22. Ibid., Figure 46.

23. Lyon, R. H., and E. Eichler, "Random Vibration of Connected Structures," J. Acoust. Soc. Am., 36, 7, 1344, July 1964.

24. Lyon, R. H., "An Energy Method for the Prediction of Noise and Vibration Transmission," 33rd Symposium on Shock and Vibration, Part II, Department of Defense, February 1964, p. 13.

25. Lyon, R. H., and T. D. Scharton, "Vibration Energy Transmission in a Three Element Structure."

26. Eichler, E., "Thermal Circuit Approach to Vibrations in Coupled Systems and Noise Reduction of a Rectangular Box," J. Acoust. Soc. Am., 37, 1965.

27. Smith, P. W., and R. H. Lyon, "Sound and Structural Vibration," BBN Report No. 1156, submitted 15 September 1964 to NASA.

UNCLASSIFIED
Security Classification

DOCUMENT CONTROL DATA - R&D

(Security classification of title, body of abstract and indexing annotation must be entered when the overall report is classified)

1. ORIGINATING ACTIVITY (Corporate author)	2a. REPORT SECURITY CLASSIFICATION
Bolt Beranek and Newman Inc. Cambridge, Massachusetts	UNCLASSIFIED
	2b. GROUP

3. REPORT TITLE

AERODYNAMIC NOISE SIMULATION IN SONIC FATIGUE FACILITY

4. DESCRIPTIVE NOTES (Type of report and inclusive dates)

FINAL 15 January 1964 to 31 March 1965

5. AUTHOR(S) (Last name, first name, initial)

Lyon, R. H. Stern, R.
Gordon, C. G. Wiener, F. M.

6. REPORT DATE	7a. TOTAL NO. OF PAGES	7b. NO. OF REFS
November 1966	69	27

8a. CONTRACT OR GRANT NO.	9a. ORIGINATOR'S REPORT NUMBER(S)
AF33(615)-1290 b. PROJECT NO. 4437 c. Task No. 443701 d.	BBN Report No. 1349 9b. OTHER REPORT NO(S) (Any other numbers that may be assigned this report) AFFDL-TR-66-112

10. AVAILABILITY/LIMITATION NOTICES

Distribution of this document is unlimited.

11. SUPPLEMENTARY NOTES	12. SPONSORING MILITARY ACTIVITY
	Air Force Flight Dynamics Laboratory RTD, AFSC Wright-Patterson AFB, Ohio, 45433

13. ABSTRACT

The possibility of simulating a turbulent boundary-layer noise environment using the air-flow capability of the RTD Sonic Fatigue Facility is investigated. The philosophy is adopted that it is the mechanical power absorbed by the structure from the environment that is to be duplicated. Calculations are developed that allow the prediction of the mechanical power injected into a structure by a turbulent boundary layer (TBL) and by a turbulent wall-jet. The possibility of replacing the power injected by the TBL by using turbulent wall-jets impinging on a structural model of a section of a supersonic transport is studied. Results indicate that high-frequency excitation (above 1 kHz) can be adequately simulated, but that the air-flow capabilities of the facility would be exceeded by an attempt to excite a structure as large as the one chosen by a set of wall-jets at lower frequencies.

DD FORM 1 JAN 64 1473

UNCLASSIFIED
Security Classification

14. KEY WORDS	LINK A		LINK B		LINK C	
	ROLE	WT	ROLE	WT	ROLE	WT
Aerodynamic noise Boundary layer Turbulent boundary layer Jets Wall-Jets Sonic fatigue Structural response						

INSTRUCTIONS

1. ORIGINATING ACTIVITY: Enter the name and address of the contractor, subcontractor, grantee, Department of Defense activity or other organization *(corporate author)* issuing the report.

2a. REPORT SECURITY CLASSIFICATION: Enter the overall security classification of the report. Indicate whether "Restricted Data" is included. Marking is to be in accordance with appropriate security regulations.

2b. GROUP: Automatic downgrading is specified in DoD Directive 5200.10 and Armed Forces Industrial Manual. Enter the group number. Also, when applicable, show that optional markings have been used for Group 3 and Group 4 as authorized.

3. REPORT TITLE: Enter the complete report title in all capital letters. Titles in all cases should be unclassified. If a meaningful title cannot be selected without classification, show title classification in all capitals in parenthesis immediately following the title.

4. DESCRIPTIVE NOTES: If appropriate, enter the type of report, e.g., interim, progress, summary, annual, or final. Give the inclusive dates when a specific reporting period is covered.

5. AUTHOR(S): Enter the name(s) of author(s) as shown on or in the report. Enter last name, first name, middle initial. If military, show rank and branch of service. The name of the principal author is an absolute minimum requirement.

6. REPORT DATE: Enter the date of the report as day, month, year; or month, year. If more than one date appears on the report, use date of publication.

7a. TOTAL NUMBER OF PAGES: The total page count should follow normal pagination procedures, i.e., enter the number of pages containing information.

7b. NUMBER OF REFERENCES: Enter the total number of references cited in the report.

8a. CONTRACT OR GRANT NUMBER: If appropriate, enter the applicable number of the contract or grant under which the report was written.

8b, 8c, & 8d. PROJECT NUMBER: Enter the appropriate military department identification, such as project number, subproject number, system numbers, task number, etc.

9a. ORIGINATOR'S REPORT NUMBER(S): Enter the official report number by which the document will be identified and controlled by the originating activity. This number must be unique to this report.

9b. OTHER REPORT NUMBER(S): If the report has been assigned any other report numbers *(either by the originator or by the sponsor)*, also enter this number(s).

10. AVAILABILITY/LIMITATION NOTICES: Enter any limitations on further dissemination of the report, other than those imposed by security classification, using standard statements such as:

(1) "Qualified requesters may obtain copies of this report from DDC."

(2) "Foreign announcement and dissemination of this report by DDC is not authorized."

(3) "U. S. Government agencies may obtain copies of this report directly from DDC. Other qualified DDC users shall request through _____."

(4) "U. S. military agencies may obtain copies of this report directly from DDC. Other qualified users shall request through _____."

(5) "All distribution of this report is controlled. Qualified DDC users shall request through _____."

If the report has been furnished to the Office of Technical Services, Department of Commerce, for sale to the public, indicate this fact and enter the price, if known.

11. SUPPLEMENTARY NOTES: Use for additional explanatory notes.

12. SPONSORING MILITARY ACTIVITY: Enter the name of the departmental project office or laboratory sponsoring *(paying for)* the research and development. Include address.

13. ABSTRACT: Enter an abstract giving a brief and factual summary of the document indicative of the report, even though it may also appear elsewhere in the body of the technical report. If additional space is required, a continuation sheet shall be attached.

It is highly desirable that the abstract of classified reports be unclassified. Each paragraph of the abstract shall end with an indication of the military security classification of the information in the paragraph, represented as *(TS)*, *(S)*, *(C)*, or *(U)*.

There is no limitation on the length of the abstract. However, the suggested length is from 150 to 225 words.

14. KEY WORDS: Key words are technically meaningful terms or short phrases that characterize a report and may be used as index entries for cataloging the report. Key words must be selected so that no security classification is required. Identifiers, such as equipment model designation, trade name, military project code name, geographic location, may be used as key words but will be followed by an indication of technical context. The assignment of links, rules, and weights is optional.